Since January 2020 Elsevier has created a COVID-19 resource centre with free information in English and Mandarin on the novel coronavirus COVID-19. The COVID-19 resource centre is hosted on Elsevier Connect, the company's public news and information website.

Materials Science & Engineering R 146 (2021) 100639

Contents lists available at ScienceDirect

Materials Science & Engineering R

journal homepage: www.elsevier.com/locate/mser

Advanced materials for personal thermal and moisture management of health care workers wearing PPE

Lun Lou, Kaikai Chen, Jintu Fan *

Institute of Textile & Clothing, The Hong Kong Polytechnic University, Hong Kong, China

ARTICLE INFO

Keywords:
PPE
Thermal comfort
Materials
Systems
Heat transfer
Moisture management

ABSTRACT

In recent years, the development of personal protective equipment (PPE) for health care workers (HCWs) attracted enormous attention, especially during the pandemic of COVID-19. The semi-permeable protective clothing and the prolonged working hours make the thermal comfort a critical issue for HCWs. Although there are many commercially available personal cooling products for PPE systems, they are either heavy in weight or have limited durability. Besides, most of the existing solutions cannot relieve the perspiration efficiently within the insolation gowns. To avoid heat strain and ensure a longtime thermal comfort, new strategies that provide efficient personal thermal and moisture management without compromising health protection are required. This paper reviews the emerging materials for protective gown layers and advanced technologies for personal thermal and moisture management of PPE systems. These materials and strategies are examined in detail with respect to their fundamental working principles, thermal and mechanical properties, fabrication methods as well as advantages and limitations in their prospective applications, aiming at stimulating creative thinking and multidisciplinary collaboration to improve the thermal comfort of PPEs.

1. Introduction

1.1. PPE and its thermal comfort issues

Personal protective equipment (PPE) is a critical component to protect healthcare workers (HCWs) from infectious hazards. In the pandemic of highly infectious COVID-19 [1], the risk of HCWs becomes a serious issue in the direct contact with patients. As reported by U.S. Centers for Disease Control and Prevention (CDC) in April 2020, about 19% of U.S. cases are HCWs [2]. Infectious pathogen such as SARS-CoV-2 (the virus that causes COVID-19) can be transmitted through 1) direct contact 2) respiratory droplets exhaled by an infectious person and 3) aerosol (smaller droplets or particles) that suspends in the air over long time [3]. For a comprehensive protection, PPE ensemble should include a surgical mask, a fit-tested respirator (N95 or FFP2), gloves, eye protection and gown or apron [4]. In a direct contact, pathogen contained liquid can transmit textile materials by either penetration through the porous structures due to the pressure gradient or permeation through diffusion due to the concentration gradient across the barrier [5]. A protective clothing (e.g., surgical gown, isolation gown or coverall) creates a barrier to eliminate or reduce contact and droplet exposure, therefore prevent pathogen transfer between patients and HCWs. The gowns with long sleeves are able to fully cover the torso and fit comfortably over the body. Standard PB70:12 from American National Standards Institute / Association of the Advancement of Medical Instrumentation (ANSI/AAMI) specifies the requirements and protection levels of protective gowns. As suggested by AAMI, HCWs who are involved in medium to high risk activities such as direct contact with blood, body fluids and other infectious materials, should wear surgical or isolation gowns [6].

To achieve high barrier resistance of water without eliminating the permeability of the protective layer, nonwoven fabrics made from spunbond/melt blown/spun-bond (SMS) (Fig. 1) polypropylene (PP) or polyethylene (PE) are most commonly used for both disposable medical gowns and surgical masks, because of the fast and inexpensive manufacturing, high levels of sterility, and effective infection control [5]. The spun bond layers can provide good thermal properties, high tear strength and good permeability, while the melt-blown layers with finer diameters can provide enhanced filtration efficiency. With an antibacterial finish, the tri-layer nonwoven fabric can be competent for Level 4 (high risk) protection in medical applications [7]. In addition to nonwovens, woven fabrics (e.g. cotton or polyester) with surface chemical finishing [8] or additional barrier membranes [9] can be applied for

* Corresponding author.
E-mail address: jin-tu.fan@polyu.edu.hk (J. Fan).

https://doi.org/10.1016/j.mser.2021.100639
Received 12 March 2021; Received in revised form 16 June 2021; Accepted 13 July 2021
Available online 2 August 2021

Nomenclature

PPE	personal protective equipment
HCW	healthcare worker
SMS	spun-bond/melt-blown/spun-bond
PP	polypropylene
PE	polyethylene
PCM	phase change material
SCBA	self-contained breathing apparatus
ITVO	Infrared-transparent visible-opaque
POTS	perfluorooctyltrichlorosilane
PDA	polydopamine
IR	infrared radiation
PEG	polyethylene glycol
UGF	ultrathin-graphite foam
PVP	polyvinylpyrrolidone
zT	figure-of-merit
AR	aspect ratio
COP	coefficient of performance
SWCNT	single walled carbon nanotubes
CVD	chemical vapor deposition
GO	graphene oxide
GOF	graphene oxide fiber
BNNT	boron nitride nanotubes
TE	thermoelectric
PM	particles matter
PU	polyurethane
PVA	poly (vinyl alcohol)
PS	polystyrene
PAN	polyacrylonitrile
PVDF	polyvinylidene fluoride
AHFD	all-hydrophilic fluid diode
TiO_2	titanium dioxide
PEI	polyethyleneimine
nanoPE	nanoporous PE
CNT	carbon nanotube
PMMA	poly (methyl methacrylate)
RH	relative humidity
FF	Fill factor
AIN	aluminum nitride
TIM	thermal interface material
MWCNT	multi walled carbon nanotube
GF	graphene fiber
LC	liquid crystal
BN	boron nitride
BNNR	boronnitride nanoribbon

reusable gowns. To ensure sufficient barrier resistance, fabrics used for medical gowns should have pore sizes less than the size of liquid-borne infectious micro-organisms [10] or be incorporated with coatings, laminates or membranes [11] for reinforcement.

The small pore size and high liquid resistance of protective gowns will inevitably impair the vapor permeability and liquid transportation during a sweating period, which will pose thermal burden to HCWs. This is because normal thermoregulatory homeostasis is disrupted by impediment of the body's heat loss to the environment [12] as a result of reduced evaporative cooling. In hot and humid environments, the risk for heat-stress-related injuries is increased greatly for HCWs who wear impermeable gown while working [13]. During Ebola outbreak in West Africa, the PPE ensembles only allowed HCWs to work for approximately 40 minutes before requiring a rest break to avoid heat stress [14,15]. Frequent donning/ doffing of contaminated PPE for rest will increase the risk of potential pathogen transmission from the PPE to the HCWs.

1.2. Personal thermal and moisture management

1.2.1. Conventional methods and limitations

Personal cooling devices such as cooling vests, which can be worn underneath protective gown during health care activities, can help reduce thermoregulatory strain and even increase working time of HCWs. Until now, the most commonly used personal cooling methods for PPE system are ice/phase change material (PCM) vests [13,16,17] and liquid cooing garments [18–20]. Coca et al. [12,13] compared different types of cooling methods (PCM vest, ice vest and liquid cooling garment with circulating semi-frozen water supply) in hot and humid environments (32 °C/92%RH) through both thermal manikin and human subject tests. They found that both the PCM/ice vests and liquid cooling garment can reduce physiological heat stress significantly for subjects wearing PPE. But PCM/ice vests have limitations in operating time [21], as the materials become warm during use thus requiring frequent donning on/off for cooler exchange. The liquid cooling garment seemed to perform better than ice/PCM vests physiologically with longer duration (4~6 hours) [21] but usually much heavier. A more important issue that undermining clothing comfort is the wetness. Due to the low surface temperature and impermeability, both PCM/ice packs and water circulating tubes inevitably facilitate moisture condensation on the cooling vests and increase the skin wetness as a result of the high relative humidity in clothing microenvironment [22]. Air cooling systems [23–25], which created ventilating air flow within the clothing microenvironment through fans or blowers can facilitate moisture evaporation, reduce the wetness and bring a significant heat dissipation. Most of the existing air cooling systems have air intake from

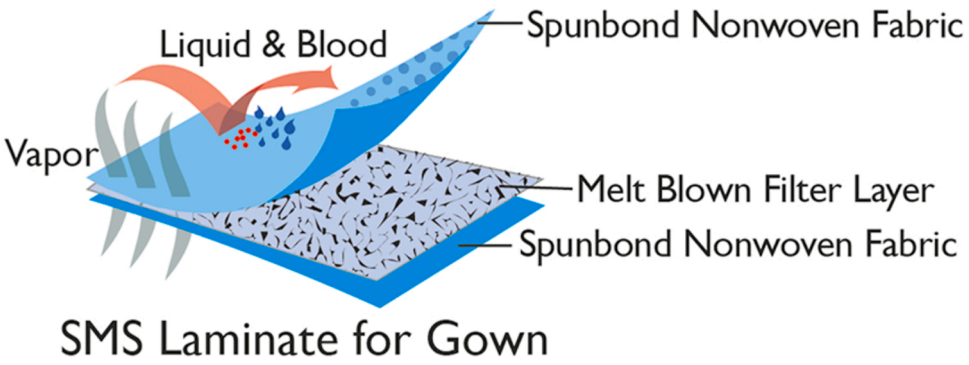

Fig. 1. Schematic illustration of SMS laminate fabric. [5]

surroundings for a lower air temperature. But this design is unpractical in the environments with highly contagious infection or hazardous micro-organisms. In addition, due to the low permeability of the PPE suit layer, the relative humidity within the clothing layer may be too high to allow an efficient evaporation of sweat under the air ventilation. Some enclosed air cooling devices such as self-contained breathing apparatus (SCBA) [26,27] containing personal ice cooling system were also applied to reduce heat stress for PPE wearers, but they are exceedingly heavy (about 20~30 kg) that result in shorter working time to exhaustion as well as lower work pace. Therefore, a lightweight and sustainable personal thermal and moisture management system which provides sufficient cooling power and reduces skin wetness without compromising the protection is highly required. However, most of the existing wearable cooling strategies have limitation in one or more aspects, therefore can't satisfy the high demand of PPE systems.

1.2.2. Advanced strategies and materials

New strategies of personal thermal and moisture management are based on the rule of human body heat balance [28] where heat loss is realized through conduction, convection, radiation and evaporation. In this article, five advanced materials are introduced in terms of their potentials in the application of thermal and moisture management for PPE systems:

1) Janus textiles with unidirectional water transport property can help remove sweat from skin surface for better thermal comfort and meanwhile prevent liquid penetration from the environment.
2) Infrared-transparent visible-opaque (ITVO) fabrics that are vapor permeable and water repellent can increase the radiative heat loss from human body for personal cooling.
3) PCM, as a conventional method for personal thermal management, can be further improved in cooling performance and wearability with the utilization of advanced encapsulating techniques.
4) Thermoelectric (TE) modules with specific design and suitable heat sinks are able to deliver a steady and sustainable cooling effect through a direct/indirect thermal contact with human skin.
5) Thermal conductive textiles, which are capable of distributing cooling power to distant areas, can realize an extensive heat absorption over human body with more uniform cooling effects.

As shown in Fig. 2, the above strategies are classified in terms of their main applications and mechanisms for the thermal and moisture management in PPE system. Janus textiles and ITVO fabrics, if produced by electrospinning, can obtain smaller pore size, large surface area to volume ratio and higher porosity, which enables them to be applied as surgical masks for aerosol/PM filtration without compromising the breathability. When being applied as protective layer of isolation gowns, Janus textiles can facilitate vapor evaporation through bringing liquid sweat to the outer surface, while ITVO fabrics enhance radiative heat loss due to the transparency to the IR radiation from human body. PCM and TE, as the cold sources, have been widely used in passive and active cooling systems, respectively. To further expand the cooling effect into large areas, thermal conductive textiles with high thermal conductivities can potentially be used together with cold sources in order to reduce the cover area of TE or PCM and cut down the total weight of clothing systems. Furthermore, incorporating blowers or fans into TE or PCM personal cooling systems can further enhance the overall cooling effects with the help of induced force convection and vapor evaporation. Generally, the advanced materials based on their applications can be classified into three aspects: protective clothing material, cold source and heat transfer media. As shown in Fig. 2, their functions in thermal and moisture management are matched with the four mechanisms of heat loss.

2. Janus textiles

Due to the low vapor permeability of conventional insolation gowns, efficient moisture management of HCWs to reduce their skin wetness becomes an urgent demand for thermal comfort. Materials that can remove moisture from skin and facilitate vapor evaporation are highly promising. Janus materials with different wettability on two sides and unique liquid management properties have attracted remarkable attentions [29–31]. A Janus textile with a gradient of hydrophilicity across the thickness can guide a unidirectional water transportation. According to Young-Laplace equation, liquid can spread into a pore if the surface of pore wall is wettable (contact angle < 90). In this condition, water tends to transport from the hydrophobic side to the hydrophilic side of the material but is blocked in the reversed direction [32,33]. In the application of insolation gowns, the property can lead to a dryer skin and a wide spread of moisture in the outer layer of the fabric for evaporation. Also, Janus textiles with porous structure can provide a higher vapor permeability that further assist the sweat evaporation without liquid penetration from the environment.

2.1. Multi-layer microporous membrane

Microporous membranes especially electrospun nanofibrous membranes have been widely studied in the application of respirator and surgical masks due to its extensively interconnected pores, variable porosity, large surface-to-volume ratio. Membranes composed of electrospun nanofibers with diameters from 10 to 1000 nm showed excellent filtering efficiency of particles matter (PM) with relatively low pressure

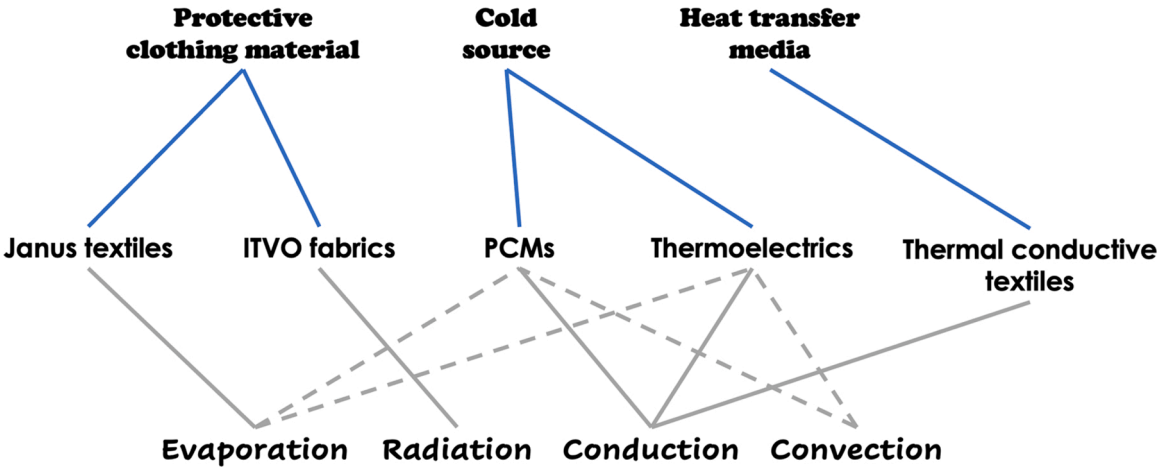

Fig. 2. Applications and mechanisms of the advanced materials in thermal and moisture management of PPE systems.

drop [34,35]. Also, the electrospun nanofibrous membrane can be endowed with superhydrophobicity [36], antibacterial property [37], protection against chemical agents [38,39] and various wettability across thickness [40]. With these properties, insolation layer can achieve a higher vapor permeability for thermal comfort and meanwhile guarantee a good protection against pathogens contained droplets and aerosols. To realize unidirectional transport of water, duel-layer membranes with two different components and structures formed independently are usually used to achieve gradient wettability. In Zhao and Jiang's work [41], a dual-layer Janus membrane composed of a hydrophobic polyurethane (PU) layer and a hydrophilic crosslinked poly (vinyl alcohol) (PVA) layer was fabricated through sequential electrospinning. Water droplet on the hydrophobic side can penetrate to the hydrophilic side within 4 seconds. In reverse direction, water droplet on the hydrophilic side spread within the layer rather than penetrating. The hydrophilic side of a fibrous membrane is considered to provide the main driving force of water transport, as water enters the inter-fiber capillary channels and is dragged along by the action of Laplace pressure. While, Lu et al. [42] found that in the hydrophobic side of a Janus membrane, polystyrene (PS) electrospun nanofibers with porous structure (Fig. 3) can also enhance the push-pull effect for directional water transport, comparing with solid PS nanofibers. They also [43] found that a core-shell nanofiber with a hydrophilic polyacrylonitrile (PAN) core inside a hydrophobic polyvinylidene fluoride (PVDF) shell can facilitate the moisture transportation from hydrophobic layer. In this study, a fluorine - rich PVDF shell of nanofiber with lubricating effect can potentially improve the tactile comfort of the fabric.

To further enhance the unidirectional transport property, Wang [44] developed a tri-layered fibrous membrane (Fig.4a) with progressive wettability by introducing a polyurethane(PU)- Polyacrylonitrile (PAN) mid-layer between hydrophilic PAN layer and hydrophobic PU layer. Compared with dual-layer membranes, an extra capillary force can be induced by the intermediate layer. As shown in Fig. 4 (c) and (d), when the droplets moved from the hydrophobic layer to the hydrophilic layer, the intermediate layer promoted liquid transport whereas hindered directional liquid transport in the opposite direction. Both the breakthrough pressure and moisture wicking performance can be improved at the interfaces of a tri-layered membrane system. In Ding's work [40], a tri-layered electrospun nanofibrous membrane was developed for PM2.5 filtration. A gradient from hydrophobic to superhydrophilic properties was created across the membrane thickness, which shows the possibility in the application of insolation gowns for aerosol protection.

Instead of creating wettability gradient, a heterogeneous geometry with gradient pore size from larger to smaller pores across the thickness can also realize unidirectional water transport. Shou and Fan [45] developed an all-hydrophilic fluid diode (AHFD) made of porous materials with asymmetric pore sizes, which allowed capillary flow in a chosen direction. A microporous membrane with pore size of 1 μm and a woven mesh with pore size of about 300 μm were stacked together, where liquid tended to spread spontaneously from the mesh side to the membrane side, because of the sudden contraction of flow path. On the contrary, a sudden expansion of flow path from the membrane side to the mesh side leaded to difficulties in water advancement. But the pore size gradient may not always guarantee a one-way fluid transport because liquid can still move from smaller to larger pores when sufficient liquid is fed from the smaller pores [46]. In real applications, microporous membranes made through electrospinning usually have poor mechanical strength due to the high porosity and weak bonding at fiber junctions [47]. Cover layers [IR83] with higher strength and abrasion resistance can be applied together with the electrospun microporous membranes for more durable protection.

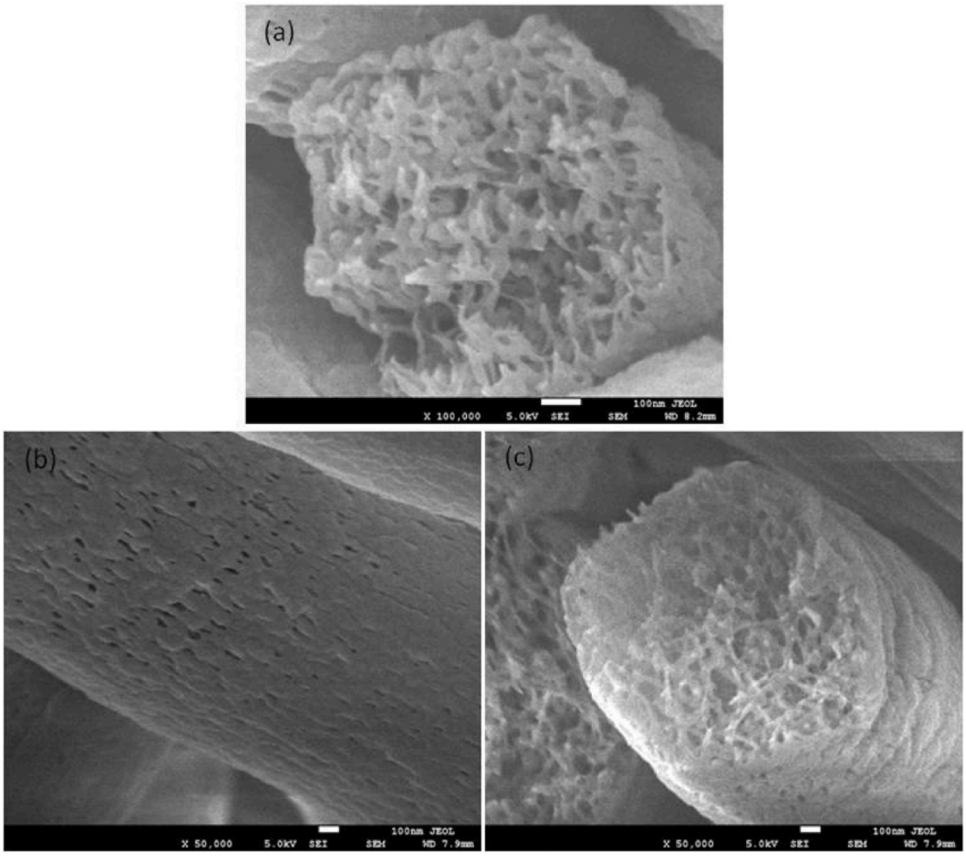

Fig. 3. FESEM image of (a) cross section of as-spun porous PS nanofibers (b) the porous PS nanofibers coated with hydrophilic coating (c) cross section of coated PS porous nanofiber. [42] Copyright 2014 American Chemical Society.

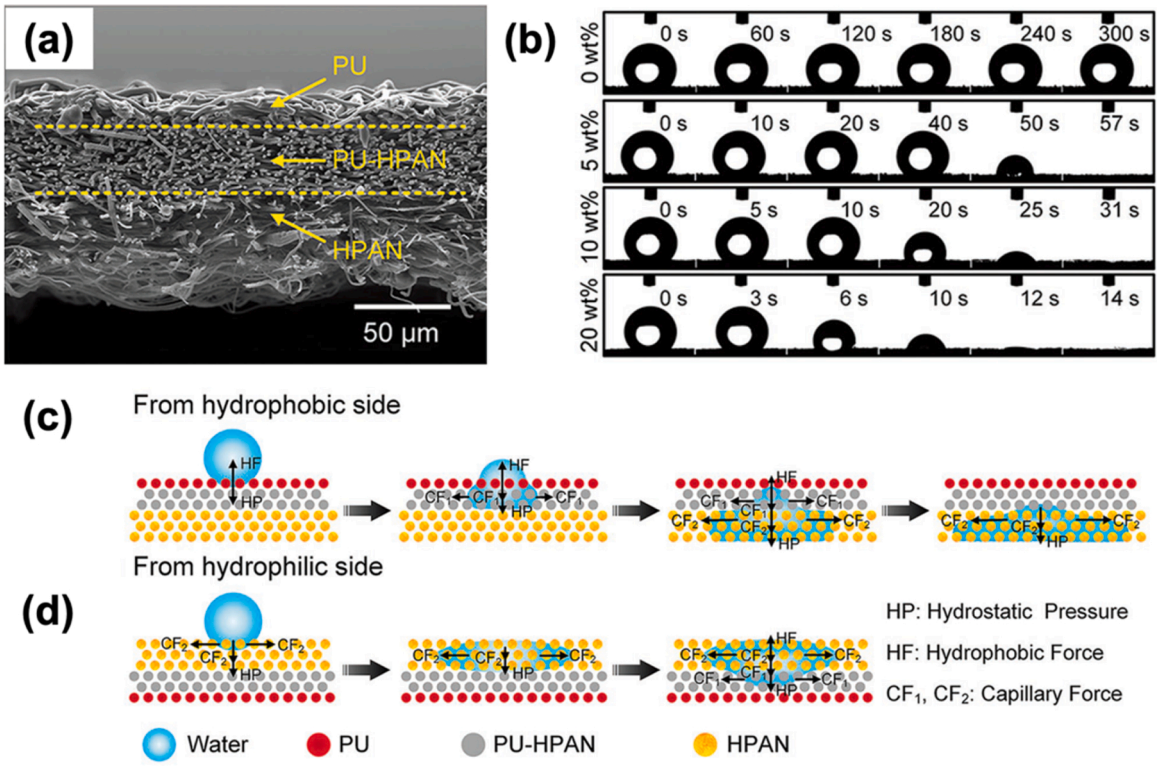

Fig. 4. (a) Cross-sectional SEM image of tri-layer PU/(PU-HPAN)/HPAN fibrous membrane (b) Water absorption property of tri-layered membranes with different concentration of HPAH. Water transport mechanism on the upward (c) hydrophobic PU side and (d) HPAN side, respectively [44]. Copyright 2018 Wiley.

2.2. Woven fabrics with surface treatment

Another strategy to achieve unidirectional water transport on protective clothing is to conduct surface treatment on traditional textiles such woven cotton fabric. Unlike microporous membranes, a woven fabric with larger pores is not able to provide efficient filtration of aerosols or small particles ($PM_{2.5}$). It was found that facemasks made of cotton/polyester blend cloth show only 40-60% filtration efficiency of aerosol particles [48]. While, cotton fabrics are commonly used in patient gowns to ensure the thermal comfort. With a unidirectional water transport property, cotton fabric can protect water droplets with potential hazardous matters from the environment and meanwhile help remove sweat from human body. Different methods have been developed to create a Janus cotton fabric with asymmetric wettability across the thickness. Tian and Ras [49] used a facile vapor diffusion method to hydrophobize one side of cotton fabric with 1H, 1H, 2H, 2H – perfluorooctyltrichlorosilane (POTS) vapor and left another side hydrophilic. Lai [50] reported an electrospraying technique to deposit SiO2 contained fluorinated superhydrophobic solution on one side of the cotton fabric for one-way water transport. The electrosprayed fabric also showed stable repellency toward various corrosive droplets including HCl and NaOH with pH of 1 and 14, respectively. The above-reported Janus fabrics can promote the transport of sweat from clothing inner side to the outer side. But the hydrophilic side of cotton fabric may have the risk of preserving liquid contaminants during storage, considering some organisms remained on fabrics can survive several months [51]. Xin [52] developed a photo-induced Janus cotton with a capability to transfer a selected side of fabric from hydrophobic state to superhydrophilic state under solar or UV irradiation with another side still hydrophobic. This technology allows a cotton cloth to keep dry and clean during storage and recover the Janus property when being used. Another drawback of Janus cotton fabric in practical use is the limited functional period. As the moisture content increases in the hydrophilic side and reaches saturation, liquid transport rate will slow down and the fabrics will become heavy and clingy. To prevent moisture saturation, Lao and Shou [53] developed a “skin-like” directional liquid transport fabric (Fig. 5a) with superhydrophobic outer surface, which repelled external water droplets and liquid contaminants. As shown in Fig. 5b, instead of making the whole piece of fabric Janus, they created “Janus channels” spatially distributed in fabric plain with a gradient wettability across the fabric thickness as a mimic of “sweating gland”. Perfluoro-coated titanium dioxide (TiO2) nanoparticles were used for superhydrophobic treatment of cotton fabric, then a selective plasma treatment via a patterned mask was applied to create porous gradient wettability channels. As shown in Fig. 5c, water droplets can be quickly transported from plasma-exposed back spot areas to top spot areas and roll-off from the superhydrophobic surface. Here, the unidirectional transport behavior can proceed smoothly even in antigravity conditions.

However, many hydrophobic treatments of cotton fabric involve the use of fluorine-containing materials, which limits the scale of industrialization due to the economic costs and environmental pollution [29]. Except cotton, fabrics/membranes made of synthetic polymers can also be used to make Janus fabrics through surface treatments. Xu [54] used a single sided polydopamine/polyethyleneimine (PDA/PEI) codeposition on a polypropylene (PP) membrane to create asymmetric wettability with the treated side significantly more hydrophilic. Lin [55] used dip-coating method to form a thin layer of superhydrophobic coating containing TiO2 and hybrid silica with hexadecyl and 3-thiol propyl groups on a polyester fabric. A subsequent UV irradiation upon one side of the fabric led to a conversion of surface chemical groups from hydrophobic to hydrophilic.

In General, Janus textiles with unidirectional water transport property show good potential in the application of medical insolation gowns. The main challenge is to provide higher moisture transport efficiency without compromising the level of protection from water droplets and aerosol penetration. Electrospun microporous membranes seem to be a promising choice when being combined with other durable fabric materials for strength enhancement. Traditional textiles such as cotton or

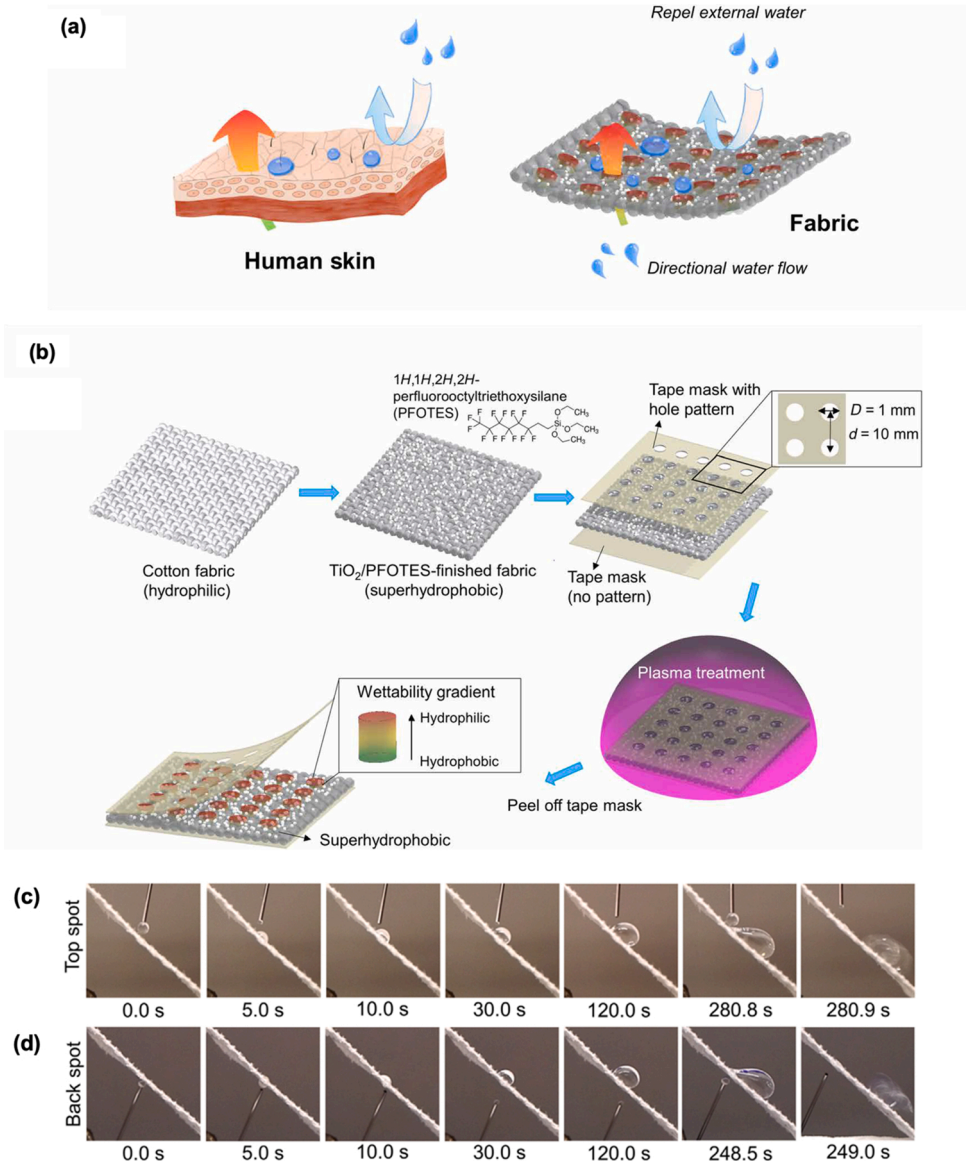

Fig. 5. (a) Schematic illustration of dual properties of the skin-like fabric (b) Fabrication process of the skin-like fabric. Still frames taken from videos when water was dropped on a inclinedly laid (45°) fabric on (c) exposed top spot areas and (d) unexposed back spot areas [53]. Copyright 2020 AAAS.

polyester woven fabrics with specific surface treatments can also help improve the moisture transport properties of medical used clothing in lower risk conditions, such as patient gowns and medical aprons.

3. Infrared transparent and visible opaque fabrics

In personal protective systems, where sweat transportation and evaporation are limited, the human body radiation that contributes to more than 50% of the total body heat loss in indoor environment [56,57] plays more significant role in maintaining the heat balance. Human skin is an effective emitter of infrared radiation (IR) with an emissivity of 0.98 [58,59]. The radiation is mainly distributed in the mid-infrared range between 7 – 14 μm, which overlaps with the transparent window of the atmosphere and therefore allows the heat to be dissipated into the outer space (3 K). When human skin temperature is around 34 °C, the theoretical net radiation power density between human body and the outer space is about 100 W m^{-2} [60]. An IR transparent clothing, using innate thermal radiative heat of human body as the cooling mechanism, has huge potential in the application of personal thermal management. While in practice, large percentage of the human body radiation is either absorbed or reflected by clothing materials, e.g. cotton and polyester, which have low IR transmittance (<0.02) [61]. Polymers such as polyethylene (PE), polycaprolactam and nylon, with simple chemical structures and fewer vibrational modes, have high IR transmittance but also are transparent to visible light (380 ~ 750 nm), thus not suitable for wearing. In 2015, Tong et al. [61] introduced a concept of infrared-transparent visible-opaque (ITVO) fabric composed of IR transparent polymers. Through a numerical study, visible opaqueness of the fabric can be realized through a structured design of fibers. With an optimized design of fiber and yarn, low reflectance (0.019) and high transmittance (0.972) of human body radiation can be obtained theoretically. In 2016, Hsu et al. [62] for the first time demonstrated the cooling function of an ITVO fabric for personal thermal management through an experimental study. They used a commercial nanoporous PE (nanoPE) film with pore sizes comparable with the wavelength of visible light as the basic material, showing a good IR-transparency and strong scattering of visible light. The weighted average transmittance for human body radiation was 96.0% (Fig. 6b) and the opacity for visible spectrum was higher than 99%. Under 23.5 °C ambient temperature, the nanoPE film showed 2.7 °C radiative cooling

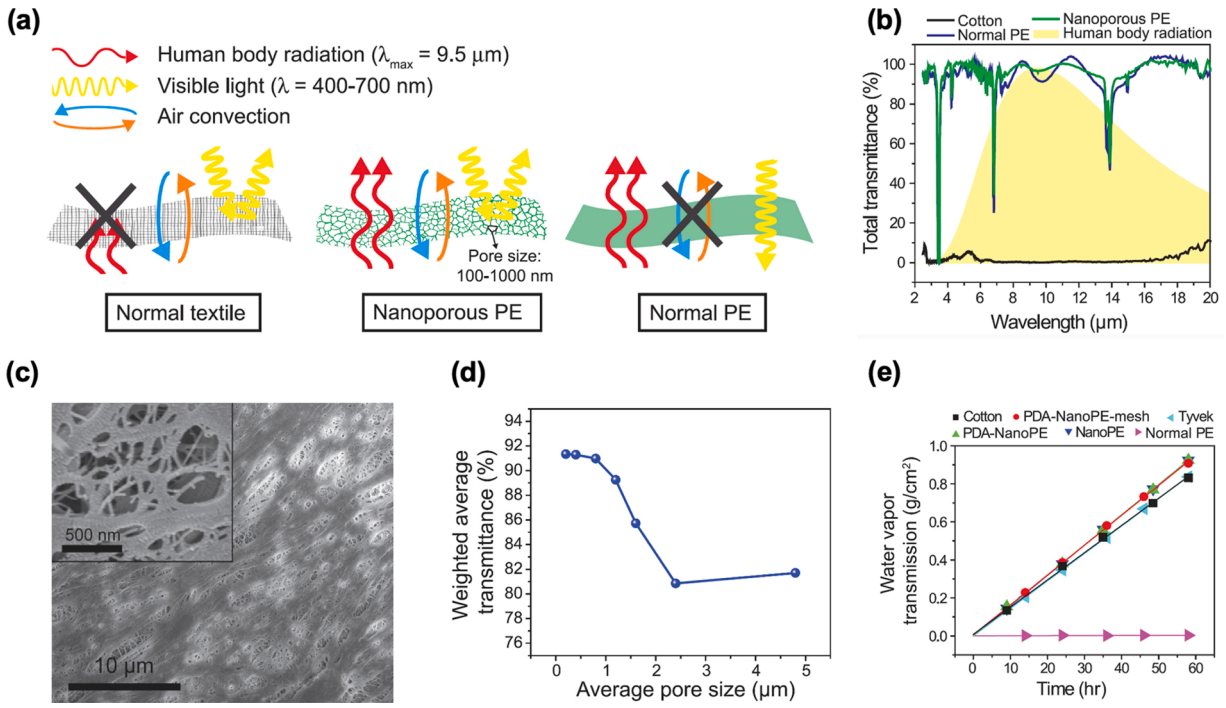

Fig. 6. Mechanism and properties of nanoPE (a) Sechematics of comparison between the nanoPE, normal PE and cotton. (b) Measured total FTIR transmittance of nanoPE, normal PE and cotton. (c) High-resolution SEM image of nanoPE. (d) Simulate weight average transmittance for various pore sizes. (e) Water vapor transmission rate test of different materials [62]. Copyright 2016 AAAS.

effect comparing with cotton fabric when a "simulated skin" with constant heat flux was used for measurement. In addition, the interconnected-pore structure and 50% porosity of the nanoPE lead to a high water vapor transmission rate (~ 160 g/m^2 per hour), which is even larger than that of a cotton fabric (~140 g/ m^2 per hour).

The good vapor transport property, hydrophobicity and small pore size (100 ~ 1000 nm) of nanoPE enables a possibility in the application of personal protection as a filtering material. But only a layer of nanoPE film is not enough to screen aerosols or particle matters (PMs) in smaller size (< 1 μm). As discussed in the previous section, a combination of nanoPE screening layer and nanofibrous membrane can realize a more comprehensive filtration of aerosol/PM in different dimensions. Besides, the nanoPE film can make up the fragility of electrospun membranes due to the good mechanical property [63]. In 2017, Yang et al. [64] developed an ITVO PM filter through transferring nylon-6 electrospun nanofibers (diameter < 100 nm) onto the nanoPE film with a total fabric

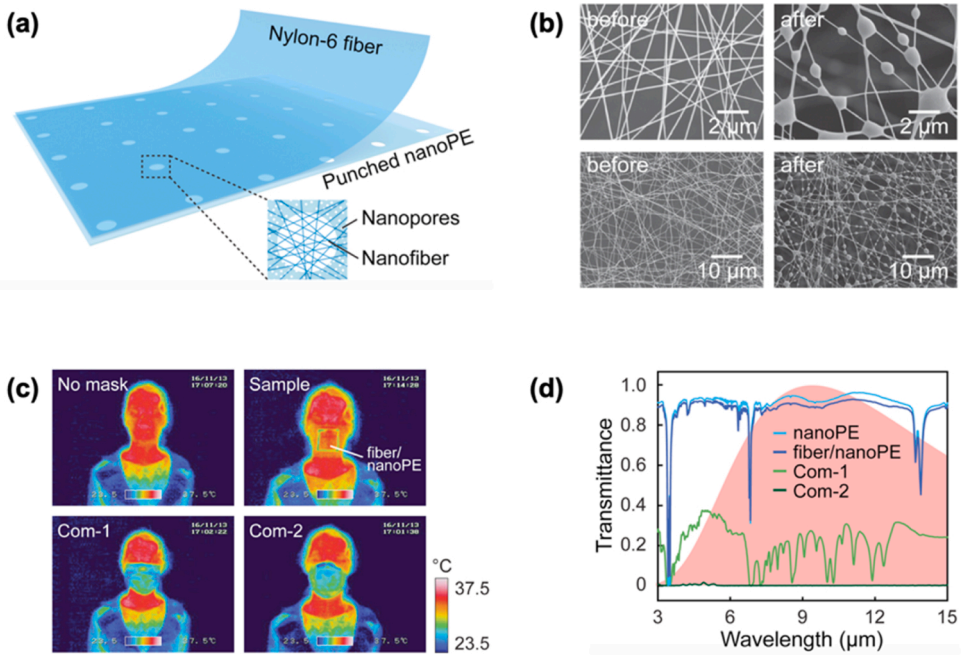

Fig. 7. Introduction and properties of Fiber/NanoPE (a) Scheme for proposed face masks with electrospun nylon-6 nanofibers on nanoPE substrate. (b) SEM images of the nylon-6 fibers before and after filtering the particle matter (c) Thermal imaging of human subject wearing different masks (Sample of fiber/nanoPE fabric and two commercial face masks, Com-1 and Com-2) [64]. Copyright 2017 American Chemical Society.

thickness of 12 μm (Fig. 7a and b). As a candidate of face mask material, the fabric showed a high removal efficiency of PM 2.5 (>99.5%) and a low pressure drop (Fig. 7c). Larger thickness of nanofibrous membrane usually leads to a higher PM filtration efficiency but may also result in lower IR transmittance due to the longer IR optical path [65]. As shown in Fig. 7d, the weight average transmittance of the nanofiber/nanoPE fabric was 0.893, much higher than that of commercial masks (0.229). In addition to the cooling function, ITVO fabrics can perform both cooling and heating functions within the same material. Hsu et al. [66] developed a dual-mode ITVO fabric through embedding a "double-face emitter", composed of a carbon layer and a copper layer, into the nanoPE film to achieve different IR emissivity (0.894 and 0.303) and reflectivity on each side of the material. The cooling and heating modes can be easily switched by turning the fabric inside out, which expands the application of ITVO face masks in different weathers. The good adaptability further enhances the potential of ITVO fabrics in the application of protective garments for personal thermal management. In particular, the nanofiber/nanoPE fabric [64] with a nylon-6 nanofibrous membrane as the inner layer and a nanoPE film as the outer layer provides good hydrophilicity for moisture absorption on the inner surface and good prevention from external water penetration.

The radiative cooling effect of ITVO fabrics has been demonstrated in indoor environment [62][64]. While, for outdoor environment under direct sunlight, the total power density of solar irradiation is about 1000 W/m^{-2} [67] and more than 60% of the total solar irradiance can be absorbed by bare human skin [60]. Even though the ITVO fabrics can scatter visible light, the solar spectrum is distributed in both visible and near-infrared ranges spanning from 0.3 to 4 μm. So, large proportion of the solar radiation can transmit through the ITVO fabric and offset the radiative cooling effect. To overcome the dilemma, Cai et al. in 2018 [60] developed a solar reflective ITVO fabric to realize personal radiative cooling in outdoor conditions. Spherical ZnO particles with diameter between 0.3 to 8 μm were mixed into the nanoPE. Due to the distinctive high refractive index and low absorption, the embedded ZnO particles enabled a selective scattering effect on visible and near-IR wavelength. As a result, the ZnO-nanoPE fabric showed a strong solar reflection (0.90) and high transmittance (0.80) for human body radiation. Besides, instead of adding particles, Song et al. [63] used electrospun nanofibrous membrane with a beads-on-nanofiber structure to enhance the solar reflection of an ITVO fabric.

Another challenge for the ITVO fabrics in the consumer market is the control of color. Commonly used organic dyes for textiles usually have strong absorption of human body radiation due to their chemical bonds, e.g. C-O, C-N, aromatic C-H, and S = O. [68,69] PE textile is more difficult to obtain colors through dyeing, because of its inert chemical property and lack of polar groups for chemical adhesion [70,71]. Cai et al. in 2019 [72] reported a colored ITVO PE textile (Fig. 8) that reflects certain visible colors, showing good color stability and negligible compromise in IR transmittance. Inorganic particles (viz. Prussian blue, iron oxide and silicon) with strong resonant light scattering effects on visible spectral range were mixed with PE for a selective reflection. The particle sizes (20 – 1000 nm) are much smaller than the wavelength of human body radiation, which guarantees a high IR transparency (~ 80%).

In general, the ITVO fabric is a promising material in the application of protective clothing or face masks for personal thermal management. Especially when sweat evaporation blocked by isolation gowns, radiative cooling effect may help enhance heat dissipation and reduce skin temperature as indicated in previous studies [62,64,72]. But for indoor conditions or when a direct radiation towards outer space is not

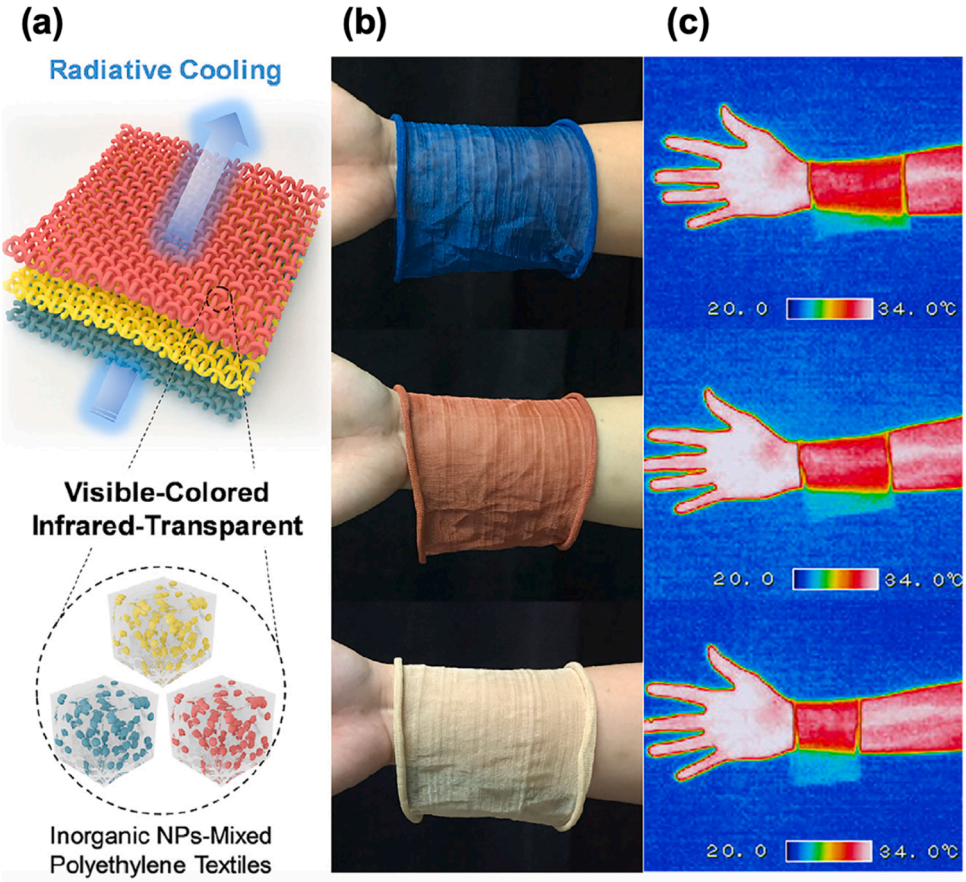

Fig. 8. Introduction and performance of the colored ITVO PE textile. (a) Design schematic for the coloration of radiative cooling textiles. (b) Photographs of the ITVO knitted textile in three different colors. (c) Infrared image of skin covered with different textiles [72]. Copyright 2019 Elsevier.

available in cloudy days, the cooling effect of the ITVO fabric highly depends on the ambient temperature. The demand for large temperature gradient may limit the application of the ITVO fabrics. Pan [73] in a numerical study showed that the heat loss through human body radiation under 30 °C is less than 50% of that under 23.5 °C, which indicates the weakening of radiative cooling effect at higher ambient temperature. Besides, the overall cooling effect of the ITVO materials as a whole garment is still not clear. More experimental studies (i.e. human subjects tests or thermal manikin tests) are required to demonstrate the overall cooling effect of ITVO clothing under different environment conditions.

4. Phase change materials (PCMs)

Phase change materials (PCMs) are thermal energy storage materials that absorb or discharge latent heat through phase transformation, which thereby renders temporary cooling or heating effects [74]. The application of PCMs for personal thermal regulation was firstly proposed by NASA in 1980s [75] through incorporating PCMs in astronauts' spacesuits for thermal protection from the extreme temperature in space. Because of the high energy storage capacity per unit weight and ease of recycling, PCM vests are the most prevalent cooling garments in the market especially for outdoor workers and people wearing PPE, to alleviate their heat strain, prolong the working time and increase the productivity. The cooling performance of PCMs depends on 1) latent heat absorbed/released 2) phase transition temperature and 3) amount of PCM encapsulated. Common types of PCM include ice, frozen gel, paraffin waxes, fatty acids, ethylene glycol and hydrated salts [76,77]. Cooling vests incorporated with ice packs [78] or frozen gel packs [79] have strong cooling capacity due to the low melting point of water but may also induce drastic skin temperature drop, vasoconstriction and discomfort sensation. Besides, freezers are always required for regeneration and storage of the ice/gel packs. Usually, for the purpose of personal thermoregulation, PCMs with phase transition temperature in the range of 18 to 36 °C are selected [80]. Paraffin-based PCMs with good chemical and thermal stability has been extensively used for clothing applications due to the suitable phase transition temperature (i.e. 18 °C to 34 °C) [81–83], high latent heat (230 – 245 J/g) [Lun] and good compatibility with various polymers. Especially the n-nonadecane, with a phase transition temperature (32.1 °C) close to human body temperature [84], is highly promising for personal cooling applications. Fatty acids [85,86], another type of organic PCM obtainable in animal fats or vegetable oils with a narrow range of phase transition temperatures, can be used as an alternative to paraffins. In addition, ethylene glycol (PEG) [87] with wide range of phase transition temperatures and large latent heat can be mixed with other PCMs for regulating the thermal properties. However, organic PCMs are generally flammable thus not applicable in personal cooling of firefighters. Inorganic hydrated salt, the sodium sulfate decahydrate (viz. Glauber's salt) [88,89], with high volumetric storage density (~350 MJ/m^3), appropriate melting temperature (32.4 ℃), high thermal conductivity and lower cost than paraffins [90] can be a better option for firefighters' cooling. But the problems of phase segregation and corrosivity of the hydrated salt PCMs limit their potentials in long-term applications.

4.1. Advance in PCM encapsulation

Solid-liquid PCMs that transform their phase from solid to liquid are commonly used in thermal management clothing. To prevent the seepage of liquid state PCM as well as the unwanted interactions with environment, techniques of microencapsulation through coacervation [91], spray-drying [92], sol-gel [93] or interfacial polymerization [94] are usually applied. However, both the PCMs and the polymer shells of microcapsules have low thermal conductivities. To improve the cooling efficiency of microencapsulated PCMs, materials like carbon nanofibers [95], carbon nanotubes [96], graphene oxide [97] or graphite nanoplates [98] can be applied to improve heat transfer performance as well as the form-stability. These additives are either coated onto the surface of PCM microcapsules [97] or dispersed into the PCMs as fillers [99]. Shi's [98] study showed that more than 10 folds increase in thermal conductivity of paraffin PCM can be achieved with the 10 wt% addition of graphite nanoplates. Increasing the loading ratio (above 10 wt%) of dispersed fillers can also help improve shape stability of PCMs but meanwhile lead to decrease in phase change enthalpy [100]. Instead of using dispersed fillers, filling PCMs back into continuous fillers, such as three-dimensional graphene sponges [101], graphene aerogels [102], or networks of carbon nanotube (CNT) [103] can further improve the thermal conductivity without undermining the phase change enthalpy. Ji et al. [104] developed a continuous ultrathin-graphite foam (UGF) that was embedded in the PCM to minimize the interface thermal resistance. As shown in Fig. 9a and b, the sponge-like porous UCF was filled by paraffin wax with a filling fraction of PCM up to 97.3 wt%. As a result, the thermal conductivity of the PCM could be increased by up to 18 times with negligible change in phase change enthalpy and melting temperature comparing with pure paraffin wax. However, such open-cell structures sometimes fail to prevent leakage of PCM at melting temperature. Ye et al. [74] applied a self-assembled 3D graphene aerogel consisting of numerous hollow cells, where paraffin PCMs can be encapsulated in the form of micrometer-scale droplets with a high filling fraction (97 wt%) (Fig. 9c and d). Due to the encapsulated structure and continuous graphene network, the composite PCM overcame the leakage problem and also delivered an enhanced thermal conductivity without compromising the phase change enthalpy. Besides the thermal conductivity, heat absorption efficiency of PCM composites is also related with the specific heat capacity and the density of materials. The specific heat capacity of PCM composites can be affected by the ratio of additives, too. In Elgafy's study [95], specific heat capacity of a paraffin wax composite decreased with the increase in mass ratio of CNTs, therefore resulting in a higher thermal diffusivity and higher heat transfer rate.

4.2. Integrating PCMs in textiles

PCMs can be integrated in textiles through packaging [105], coating [106], printing and padding [107]. In Bennett's study [79], a cooling vest incorporated with frozen gel packs could help reduce human body core temperature by 0.9 °C in a warm and humid condition, which was equivalent to 26.1 W/m^2 heat absorption. Despite the high cooling capacity, garments with PCM packs are usually heavy and bulky [108,77]. For the methods of coating, printing and padding, PCMs are usually encapsulated in protective shells and integrated in conventional textiles (e.g. cotton [109,110] or polyester [111,112]) by filling up the micropores of fabrics, which inevitably undermines the air permeability. Besides, the binding between PCM microcapsules and textile materials can reduce the softness of the fabric. Therefore, a sacrifice in wearing comfort of the textiles is usually involved in the utilization of above methods [86].

Instead of adding components to conventional fabrics, integrating PCMs into fibers can realize heat absorption without adding weight or compromising air permeability of fabrics. The PCM contained fibers can be achieved by blending PCM in solutions [113,114], adding PCM nanocapsules [115] or using coaxial spinneret [116] in the spinning process. Usually, PCM contained fibers are produced by solvent spinning rather than melt spinning because the melt state of PCM powers may lead to an aggregation and degradation [117]. Compared with other methods, coaxial electrospinning, which produces core-sheath structured ultrafine fibers with PCMs encapsulated inside, seems more promising in providing strong and uniform cooling effect due to the continuous encapsulation of PCMs over the structure of fibers, good physical properties, high loading ratio of PCMs and high phase change enthalpy [118]. Lu et al. [119] reported a paraffin-loaded core-sheath nanofibers through encapsulating paraffin wax into Poly(methyl methacrylate) (PMMA) with solution coaxial electrospinning method

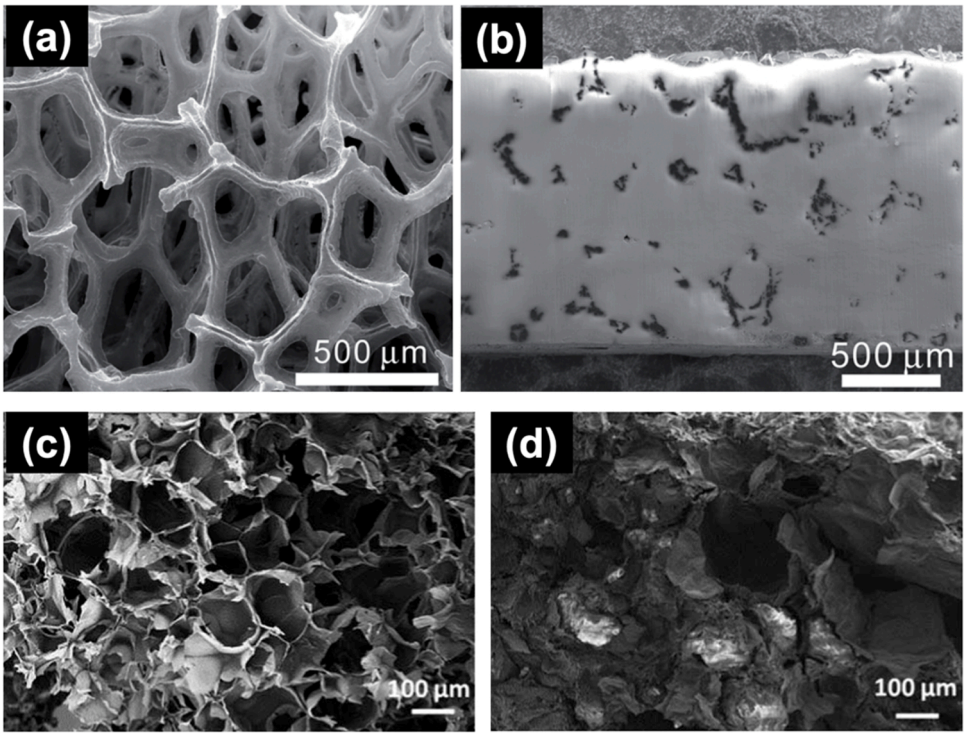

Fig. 9. SEM images of UGF (a) before PCM filling and (b) filled with paraffin wax [104]; SEM images of graphene aerogel (c) before PCM filling and (d) filled with paraffin [74].

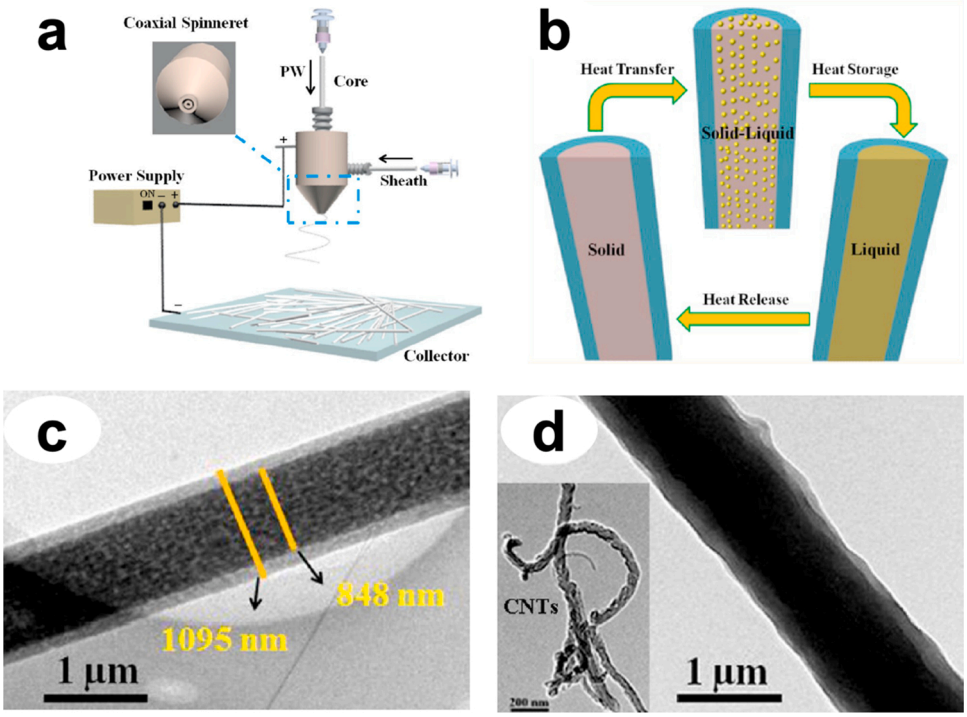

Fig. 10. Introduction of the paraffin-loaded core-shell nanofibers with PMMA sheath. (a) Schematic illustration of the coaxial electrospinning technique (b) Heat stored process of the core-sheath nanofibers (c) TEM images of core-sheath nanofibers without CNTs. (d) TEM images of core-sheath nanofibers with 10 wt% CNTs added in PMMA [119]. Copyright 2018 American Chemical Society.

(Fig. 10). It was found that higher feed rate of core material results in higher encapsulated content of PCM. With an optimal feed rate and concentration of the core material, PCM core-sheath nanofibers with high flexibility, high latent heat (57.65 J/g), good mechanical strength, large specific area was achieved. The sheath material helped maintain the shape of fiber and prevent leakage of PCM melt. However, even though CNTs were added in PMMA sheath, no significant improvement in thermal conductivity was observed because of the strong influence of

phonon scattering on amorphous polymers [120]. In Haghighat's work [118], a PCM/Polyvinylpyrrolidone (PVP) core-sheath nanofiber with 36% encapsulation ratio of PCM and 80 J/g phase change enthalpy was developed. In a simulating study, at the melting point of PCM, the surface temperature difference between PCM/PVP core-sheath samples and pure PVP samples could be 10 °C, which indicates a good potential of core-sheath PCM fibers in the application of thermal management. It was also found that reducing the sheath feed rate and keeping core feed rate can help reduce the wall thickness of sheath and increase the loading ratio of PCM.

Although the air permeability of PCM textiles can be improved, in the hot environment [225] [226], moisture condensation and sweat accumulation may occur on the surface of PCM garments due to the high microclimate RH inside PPE as a result of continuous sweat production and relatively low surface temperature of PCM. This may counteract the cooling effect and undermine thermal comfort. To solve this problem, hybrid cooling vests combining PCMs with ventilating fans [121] or desiccants [122] were developed for moisture removal. In Itani's study [123], different types of PCM cooling vest were investigated under various ambient conditions. It was found that the PCM-Fan vest is effective in low and moderate RH conditions, while in high RH conditions, the PCM-desiccant vest is recommended. But these additional components further increase the weight of the PCM cooling garments. Dorman [124] claimed that PCM cooling garments less than 1.5 kg are preferred for minimal effect on human metabolism. To meet the requirement of ASTM F2371-16 standard (viz. 50 W cooling power for more than 2 hours at 35 °C/40% RH), the weights of commercial PCM/ice vests are commonly up to 1.8 ~ 3.5 kg.

In general, PCMs with high heat absorption efficiency, adjustable phase transition temperature, replaceable cooling source and good adaptability to various environments are highly promising for the application of personal thermal management. The working performance of PCM cooling vests is related to the material type, filling ratio and distribution. However, there is always a tradeoff between the working performance and the wearing comfort [117]. Longer duration and higher cooling capacity usually come together with larger weight, lower flexibility, larger cover area and reduced air permeability for PCM cooling vests. Core-sheath nanofibers with PCM encapsulated inside have good potential in obtaining large loading ratio and secured encapsulation of PCMs without compromising thermal comfort properties of textiles. But due to the low thermal conductivity of sheath materials, the phase transition enthalpy is usually lower than that of pure PCMs, thus undermining the cooling capacity. Therefore, the encapsulation of PCMs with good compatibility in textiles, high thermal conductivity, high phase transition enthalpy and no seepage needs further investigations and explorations. In addition, a heat transfer media with high thermal conductivity and good compatibility with apparels can be applied together with PCMs to spread the cooling effect to larger areas of human body with more uniform heat distribution. It can potentially reduce the weight of clothing systems through using less amount of PCMs with lower phase transition temperature, which was considered to cause overcooling and discomfort during a direct contact with human body.

5. Thermoelectric systems

Thermoelectric (TE) cooling materials are solid-state heat pumps based on Peltier effect [125–128]. A TE module consists of several thermocouples, which are comprised of p- and n- type TE materials, connected electrically in series and thermally in parallel [129]. With electric current applied, charge carriers (electrons and holes) in TE module carry the heat from one side to the other and the thermocouple junctions are heated or cooled depending on the current direction, thus allowing heat exchange between the TE and surroundings. TE coolers have been widely used for heat management and precise temperature control of small and portable systems such as automotive air-conditioner [130], electronics [131] and medical devices [132] etc., due to the advantages of being lightweight, noiseless, highly reliable, long lifetime, no chemical reaction or emission and low maintenance requirement [133]. Recently, the TE coolers with small size and adjustable cooling effects have drawn a lot of attention in the application of wearable devices for personal thermal management [129,134,135]. To achieve sufficient cooling effect of a TE module, the Peltier cooling power on the cold side must overcome the heating effects of both joule heating and the heat conduction from the hot side, which demands the use of heat sinks for efficient heat dissipation. Besides, the microscopic surface roughness of TE module and heat sinks may result in asperities between two mating surfaces. These asperities lead to poor thermal conductivity because of the air gap in between and bring challenges to heat transfer. Therefore, the improvement of a TE cooling system can be realized in four aspects: 1) TE module performance 2) heat rejection of heat sinks 3) compatibility of different components 4) interfacial thermal conductivity.

5.1. Advance in TE module

The performance of a TE module is determined by both material types and design parameters. It can be quantified with a dimensionless metric, figure-of-merit (zT) which indicates that higher Seebeck coefficient, higher electrical conductivity and lower intrinsic thermal conductance are favorable for greater cooling effects [136]. In the past decades, different types of TE materials, such as metal chalcogenides, silicides, skutterudites, zintl phases, clathrates, metal oxides and organic semiconductors, etc. have been developed [133]. Among these materials, Bismuth chalcogenide Bi_2Te_3 and its alloy, most notably $Bi_{2-x}Sb_xTe_3$ (p-type) and $Bi_2Te_{3-x}Se_x$ (n-type), [137–139] are the most suitable choices for the temperature range for human activities. In such conditions, the hot side temperature of TE is typically limited to less than 250 °C in order to avoid decline in zT and material instability [140]. Recently, new materials like $Bi_{0.5}Sb_{1.5}Te_3$ has been reported to show a zT up to 1.9 at 50 °C with grain boundary dislocations induced [141]. On the other side, design parameters of TE module such as fill factor (FF), aspect ratio (AR) of TE pillars, etc. also play important roles in determining the performance of TE. In the application of wearable devices, Suarez [142] found that TE modules with FF lower than 20% are more suitable for on-body use. Due to the poor thermal conductivity (0.3 W/mK) [143] and limited heat flux [144] of human skin, TE in a body-contact condition will go through a low heat load and high thermal resistance, which increase the challenge in achieving high cooling efficiency. Commercial TE coolers usually have FF greater than 25% and AR around 1.0 that are less favorable for on-body use. Kishore [129] developed a wearable TE cooler (Fig. 11), with optimized design of FF and AR, capable of cooling the human skin 8.2 °C below the ambient temperature. As shown in Fig. 11b, the optimum FF for wearable TE cooler should be less than 15% and the optimal AR should be in the range of 1-2. It was also found that under high-thermally resistive environment, such as deployment on human body, lower thermal conductance of TE module is more influential than higher Seebeck coefficient. Since the cooling effect is limited within the contact area, to achieve sufficient cooling power (23 W at 26 °C) for human body [134], about 300 cm^2 contact area is required for this TE cooler. Therefore, as a wearable device, a flexible TE is necessary to allow free body movement and good tactile comfort.

However, conventional flexible TE materials made of polymers or hybrids of organic/inorganic materials usually have low figure of merit [133]. Hong et al. [135] developed a flexible and effective wearable TE cooler (Fig. 12) with rigid inorganic high-zT TE pillars sandwiched between stretchable elastomer Ecoflex sheets. Tall pillars were applied to provide larger air gap and small thermal conductance between cold and hot side of the TE cooler, resulting in a higher zT. But the tall pillar also brought larger electrical resistance, greater joule heating and lower flexibility of material (Fig. 12e). Therefore, an optimal height of pillar was selected to achieve a high zT as well as a balance between thermal

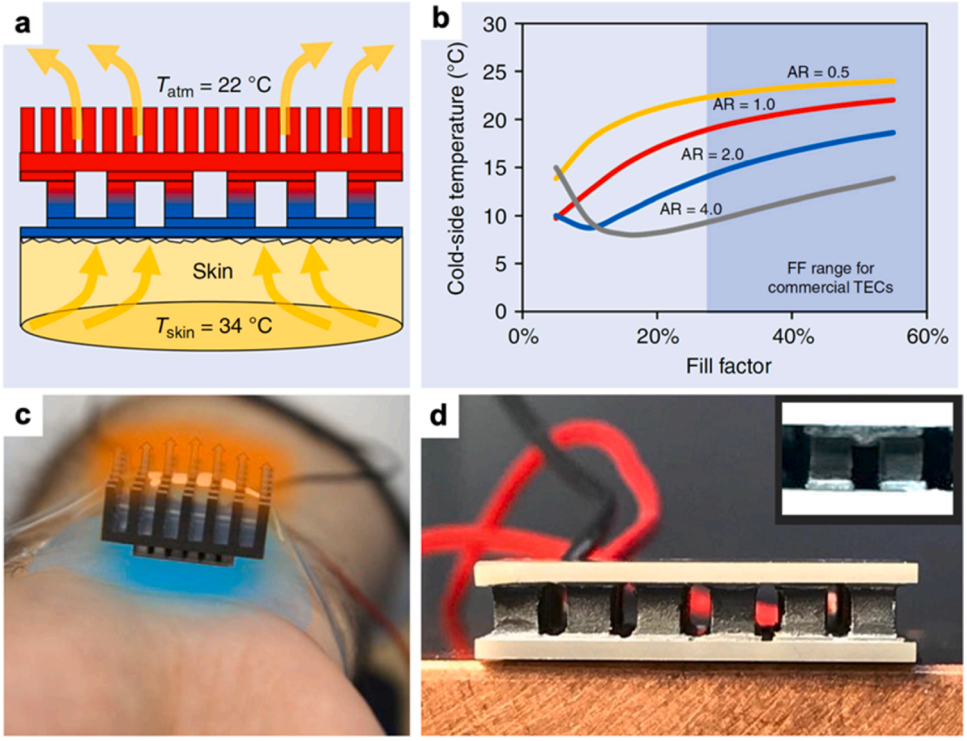

Fig. 11. (a) Schematic illustration of the wearable TE cooler. (b) Cold-side temperature of the wearable TE cooler at different FF and AF. (c) Wearable thermoelectric cooler provides localized body cooling. The arrows illustrate heat flow from human body to the ambient via TE and heat sink. (d) Thermocouples, comprising of p- and n- type legs, in the TE module [129]. Copyright 2019 The Author(s).

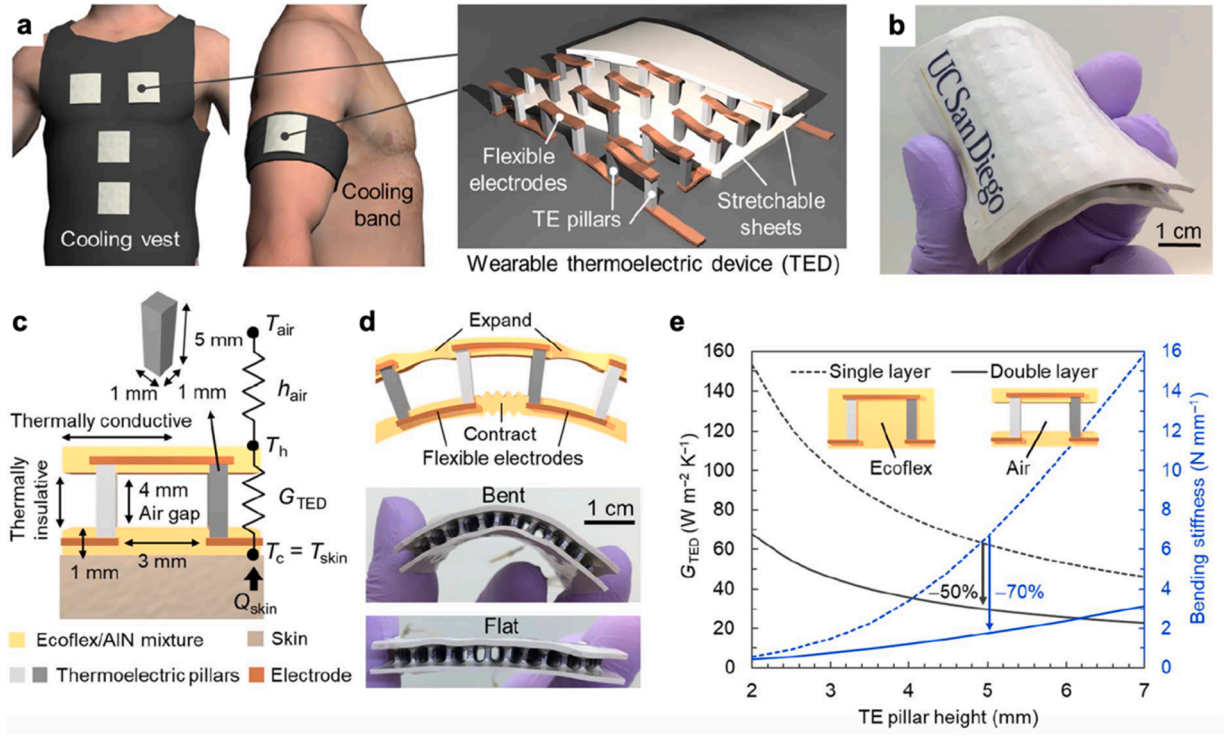

Fig. 12. Design and fabrication process of flexible TE cooler; (a) Schematic illustration of cooling garment with flexible TE coolers (left) and internal structure of TE (right); (b) Photograph of flexible TE cooler; (c) Schematic illustration of TE design, where h_{air} is heat transfer coefficient, G_{TED} is thermal conductance, T_h and T_c are temperatures at hot and cold sides of TE; (d) Schematic diagram and photographs showing the flexibility of the TED; (e) Finite element simulation of G_{TED} and bending stiffness of flexible TE coolers as a function of pillar height [135]. Copyright 2019 AAAS.

and mechanical properties. In addition, to enhance the in-layer thermal conductivity of the flexible layers, Aluminum Nitride (AIN) microparticles were added into the Ecoflex sheet. As a result, the TE cooler with a high AR (5.0) and low spatial density (6.25%) showed a zT of 0.71 at room temperature. Without using heat sinks, the flexible TE cooler was able to reduce the local skin temperature by 2.5 °C under 36 °C ambient temperature.

5.2. Improvement of TE systems

High zT of TE module along does not guarantee a high cooling power. In terms of optimizing the cooling performance of a TE system, heat resistance of the heat sinks on hot and cold sides of TE could be a more dominant factor. [145] The most commonly used heat sinks in the market are made of aluminum or copper due to the high thermal conductivity and good machinability. To further improve the heat dissipating efficiency, a lot of numerical studies have been devoted to the optimization of heat sink structure for minimal thermal resistance. It was shown that theoretical analysis with the heat balance equations of heat sinks can provide a reasonable prediction of real performance of TE cooler [146]. In practice, there are two common types of heat sinks: plate-fin heat sinks and pin-fin heat sinks. The former offers simple design and easy fabrication, while the latter has larger surface area for heat exchange and higher production cost. Kim [147] found that under impinging flow conditions, the heat sinks with pin-fin structure performed better than those with plate-fin structure. Also, the heat sinks with dense fin structure had better performance than those with loose fin structure. In Seo's work [148], influence of heat sink structure on the performance of TE cooler was investigated under a duct flow condition. For plate-fin heat sinks, increasing the fin thickness and fin number can improve heat dissipating rate significantly on the hot side, while the increase in bottom thickness has little influence on the heat dissipating rate.

In addition to the design of each component (TE module, heat sinks), the degree of compatibility among different components in an integrated TE system also influences the optimum performance. Zhou [149] proposed an optimal allocation of thermal resistance between cold side and hot side in a TE cooling system. The optimal ratio (cold side to hot side) is 1.13 ~1.50 for maximum cooling capacity and is 0.96~1.22 for optimum coefficient of cooling performance (COP). Zhu et al. [150] discussed the optimal allocation ratio of heat transfer area for heat sinks at hot and cold sides. They also proposed the optimum configuration of plate-fin heat sink for minimum entropy generation [151]. Lu [145] found that the optimal thermal resistance of TE module should account for 40-70% of the total thermal resistance in an integrated system. Based on these findings, Zhao et al. [134] and Lou et al. [152] reported a wearable thermoelectric air-cooling/heating system (Fig. 13) that blows cool or warm air to different locations of human body for personal thermal management. In this system, a pin-fin heat sink with impinging flow was applied on air rejection side for heat dissipation and a plate-fin heat sink with duct flow was used on the air supply side for cooling/heating (Fig. 13c). Also, a relationship between thermal resistance and weight of heat sink was established for the optimal design. In the cooling mode, the system was able to provide 15.5 W cooling power to human body at 26.1 °C ambient temperature through a forced convection.

The thermal conductivity at the interface between TE and heat sinks also plays an important role in determining the overall heat transfer efficiency. The actual contact area of two mating surfaces can be only 1-2% of the apparent contact area due to the surface roughness [153]. To enhance the thermal coupling, thermal interface materials (TIM) are usually applied at the interface between two contact components. Here, soft materials are preferred as they can conform to the surface textures under pressure [154]. There are three main types of TIM: 1) Carbon-based materials such as carbon nanotubes (CNTs) or graphene [155–157], 2) Metal-based materials such as solders and low melting temperature alloy [158–160], 3) Filler-based materials such as pastes, epoxies, adhesive [161–163]. Except using TIMs, Karwa [164]

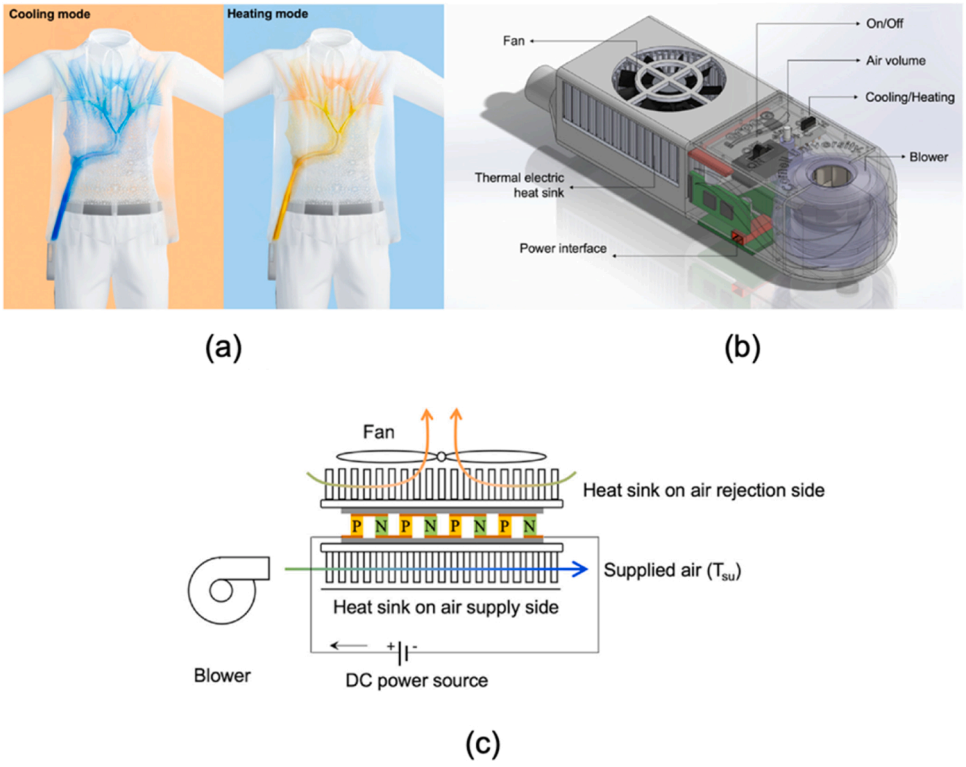

Fig. 13. (a) Illustration of the design and functions of the wearable thermoelectric air cooling/heating system; (b) 3D perspective of the air supply unit with TE, heat sinks, blower and control system integrated; (c) Schematic illustration of the air supply unit [152]. Copyright 2020 Elsevier.

developed a water jet cooled heat sink, which deployed a direct contact between water flow and TE module surface for heat exchange. A low thermal resistance (0.025 K/W) on the hot side can be achieved due to the eliminated interfacial thermal resistance.

Compared with passive methods (e.g. Janus textiles, ITVO fabrics or PCMs), the TE cooling device as an active method has advantages in providing stable and adjustable cooling power. For on-body applications, TE coolers with an optimized material design [129,135] can deliver a strong cooling effect. Also, the TE cooling systems can be made in smaller size [129,135] and lighter weight than PCM cooling vests or liquid cooling garments. But the distinct temperature drop of local skin area may occur and result in local thermal discomfort when the TE coolers are in direct contact with the human body. Expanding the contact area of TE coolers will block the sweating evaporation from human body just like PCM packs. TE air cooling systems [134] [152], which can provide both convective cooling and evaporative cooling effects, shows a great potential in the application of personal thermal and moisture management. However, the hot side of a TE cooling system usually needs to be exposed to the ambient air for an efficient heat dissipation, which may increase the risk of exposure for personal protective systems. Since the cooling efficiency is highly dependent on the ambient temperature, it makes the TE cooling system less efficient in hot environment or being used inside PPE microclimate. Besides, the use of battery may further increase the burden of heat dissipation when batteries need to be placed inside PPE microclimate. Therefore, to realize a sufficient heat dissipation and thermal comfort without compromising the protection and wearability of the whole PPE system, innovative methods on both TE system and PPE design are required. A system with the TE cooling device detachable from the garment is preferred for more convenient washing.

6. Thermal conductive textiles

6.1. Introduction and traditional methods

Thermal conductive materials, which take up heat readily from the environment, have good potential to be applied in personal thermal management when being integrated into textiles or clothing [165,166]. They can help facilitate the body heat dissipation or distribute the cooling effect generated from the cold sources (e.g. PCM or TE) to larger body areas as a heat transfer media.

At present, metals such as gold [227], silver [228], copper [229], stainless steel [230] and aluminum [231,232] have been incorporated into textiles for conducting electricity and radiation shielding. The presence of metal in textiles also improved their properties in thermal conduction and heat dissipation. To combine them with traditional textile materials, metals can be fabricated into pure metallic fibers [233], multistrand metallic wires [229,234], braiding metallic yarns [235,236] or metal-coated compound yarns [237–239]. Metallic fibers or yarns are usually woven or knitted into fabrics. In Liu's study, a knitted heating fabric was developed through combining silver plating compound yarns with staple fiber spun yarns [228]. However, metallic textiles usually have large friction force and weak cohesive force, which may lead to slippage or separation in the spinning process [240]. Also, the low elastic recovery rate and low bending resistance of fine metallic fibers may even result in breaking and falling off from the fabric. For metallic coated fibers or yarns, the coating on the surface may undergo a damage during the washing process [241].

To avoid these problems and further improve the cooling effect of thermal conductive textiles, some new and promising thermal conductive materials, including carbon nanotube (CNTs) fibers, graphene fibers and boron nitride materials will be introduced in this section. These materials will be discussed in their fundamental principles, thermal and mechanical properties, fabrication methods, and potential in textiles applications, along with the perspectives and challenges.

6.2. Carbon nanotube fibers

Carbon nanotubes (CNTs) have attracted much attention in the field of nano energy and electronics due to their high electron and phonon transport ability as well as good compatibility with nano-scale devices. Carbon nanotubes have a cylindrical structure, which is made of twisted flake graphite with different layers. According to the layer number (Fig. 14), CNTs are divided into single walled carbon nanotubes (SWCNTs) and multi walled carbon nanotubes (MWCNTs). It is reported that the maximum thermal conductivity of CNT can be 3000 W/m·K [167] and the minimum achievable diameter of SWCNTs is around 0.4 nm due to the strain limitations, with length up to 3 mm. Up to now, arc discharge [168], laser ablation [169] and chemical vapor deposition [170] are three main strategies used for producing carbon nanotubes. In addition, electrolysis [171] and solar energy [172] methods have also been proposed. Depending on the carbon source (aromatic or non-aromatic), catalyst composition and operating conditions (temperature and pressure), the composition of CNTs as well as their length and chirality could be adjusted [173]. It is desirable to understand the sensitivity of these parameters to the properties of CNTs because they have a great influence on the formation of macro components such as CNT fibers. The good performance of macromodule is attributed to the advantages such as long length and excellent arrangement of carbon nanotubes. In addition, it is very desirable to fill CNTs in a defect free arrangement.

In recent years, an important advancement in CNT technology is the development of spun CNT fibers. CNT fibers consist of millions of quasi-parallel aligned nanotubes with high mechanical strength, extraordinary structural flexibility, high thermal and electrical conductivities, novel corrosion and oxidation resistivities, and high surface area are highly promising for wearable textiles. The integrated features of the giant inter-tube contact area and the large aspect ratio of CNTs guarantee a distinguish mechanical strength of CNT fibers (tensile strength of 300 MPa and Young's modulus of 40 GPa) [174]. Unlike conventional strong carbon fibers, CNT fibers also have good structural flexibility. The tensile strain at failure is normally lower than 20% for straight CNT fibers but can be as high as 285% when fibers are coiled [175]. These features enable the CNT fibers to be integrated into textile by weaving or knitting. Furthermore, the theoretical maximum density of closely packed CNT fibers depends on both the diameter and the number of graphitic shells of individual nanotubes. The maximum density is 1.0-1.4 g/cm^3 for the nanotubes with 4-6 nm diameters and 2-3 layers of wall and is 1.5-2.0 g/cm^3 for those with 8-11 nm diameters and 6-10 walls [176]. Due to the non-perfectness of nanotube alignment, most reported fiber densities are lower than those of cotton yarns (1.55 g cm^{-3}) and polyester fibers (1.38 g cm^{-3}) [177,178], which indicates an advantage of lightweight in textile applications. Since CNTs in applicable scale are normally within several millimeters, it is important to assemble CNTs without accumulating joint defects along the fibers.

For the fabrication of CNT fibers, different approaches have been developed, including wet spinning of fibers from a CNT solution [179], dry spinning of fibers from either a drawable nanotube forest [180] or a floating catalytic chemical-vapor-deposition zone [181]. Inspired by the widely used coagulation spinning for polymer fibers, continuous CNT composite fibers have been prepared by extruding a CNT aqueous solution dissolved with the assistance of surfactants into a flowing polymer solution. Behabtu et al. [179] demonstrated that the fibers obtained from CNT Chlorosulfuric acid solution through wet spinning had high thermal conductivities (380 W/m K) and high mechanical performance (average tensile strength of 1 GPa and average Young's modulus of 130 GPa). Like the traditional technique used for spinning cotton yarns, CNT fibers can also be spun in a dry state from nanotube reservoirs as spinnable nanotube arrays or floating nanotube aerogel webs. Spinnable nanotube forests, which are synthesized by chemical vapor deposition (CVD), can be transformed into a continuous, horizontally aligned nanotube sheet by a simple dry drawing method [182]. Then, adding

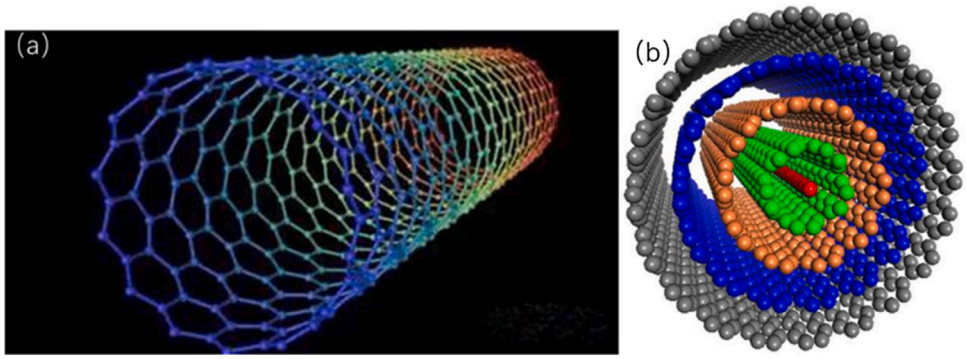

Fig. 14. Structure diagram of carbon nanotubes; (a) single walled carbon nanotubes; (b) multi walled carbon nanotubes [167].

twists at the beginning of the sheet during drawing can transform the sheet to a yarn. An aerogel thin web of CNTs can also form by injecting a catalyst-containing carbon-source solution in a high-temperature CVD reaction tube furnace. Subsequent processing of the flowing web either by twist-spinning or by liquid densification produces a continuous CNT fiber. Unlike the wet-spinning process, the dry-spinning process does not involve complicated nanotube dispersion and purification processes, which may induce structure damages to CNTs, thus can retain some important intrinsic properties, such as large aspect ratio, high electrical and thermal conductivities, and high mechanical performance, of individual nanotube. Adjustable structures and properties for dry-spun fibers are enabled by controlling the spinning process and growth conditions as well as broadening the applications of fibers for various targets. While the CNT fibers from spinnable forests have better nanotube alignment and fewer impurities than aerogel-based fibers. Aerogel-based fibers are more reliable for mass production due to the good fiber-spinning continuity and the lower-cost catalyst deposition.

Baughman's group [183] developed a multifunctional composite fiber composed of CNT sheets and functional guest materials by the biscrolling technique (Fig. 15a-c). Such multifunctional CNT composite fibers with a low concentration of CNT had good flexibility and durability (Fig. 15c) that can potentially be integrated into textiles through weaving or knitting. As shown in Fig. 15d-j, the CNT multifunctional composites fibers were made into yarns and fabrics for the purpose of artificial muscles, wearable electronics, etc. that further demonstrates the potential to be applied in wearable textiles.

In terms of industrialization, both the wet-spinning and dry-spinning techniques can be scaled up for mass production of CNT fibers. Wet spinning is more compatible with existing techniques in industry, which was used for producing polymer fibers. Pasquali's laboratory at Rice University [179] has demonstrated a successful production of several hundred meters long CNT fibers at high extrusion rate (600 m/h) with 1

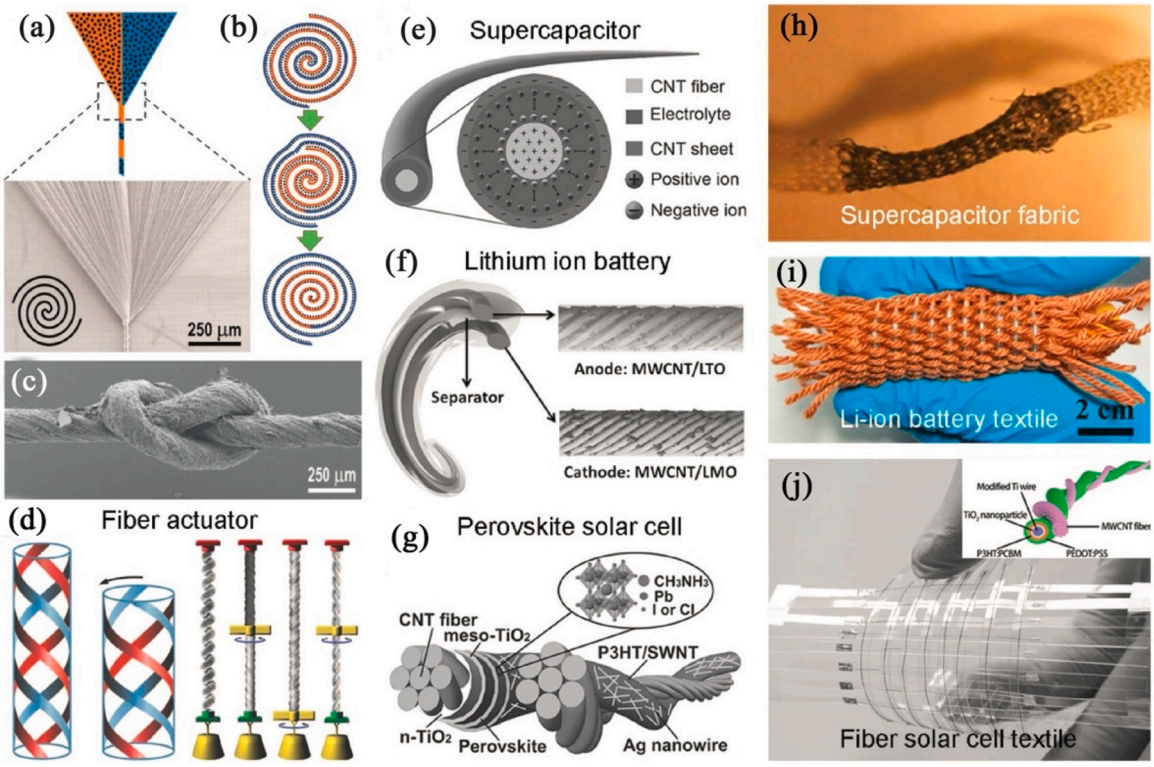

Fig. 15. (a) and (b) Schematic diagram of the biscrolling technique for the fabrication of CNT composite fibers; (c) SEM image of the CNT/SiN composite fiber [183]; (d) Mechanism of the torsional and tensile actuations induced by volume expansion [184]; (e) Schematic diagram of cross-sectional structure and working mechanism of the coaxial fiber supercapacitor [185]; (f) The structure of flexible fiber lithium-ion battery [186]; (g) Fiber solar cell consisting of two-ply CNT fibers [187]; (h) Knitted tubular fabric supercapacitor containing CNT [188]; (i) Textile knitted fibrous lithium-ion batteries containing CNT in both anode and cathode [189]; (j) A solar-cell textile with CNT fiber as the cathode [190].

to 19 fibers extruded simultaneously. DexMat company has tried to commercialize such wet-spun CNT fibers [191]. For the dry spinning technique, companies like Nanocomp Technologies, Inc. [192], Q-Flo Limited [193], Tsinghua-Foxconn NanotechnologyResearch Center, and Suzhou CreativeNano-Carbon Co. Ltd. [194] have realized the mass production of CNT fibers. Today, commercially available CNT fibers in some circumstances can replace copper wires due to the lightweight and excellent mechanical properties. In addition, CNT fibers have a surface area of 100–500 m^2/g depending on the structure of the nanotube constituent [195]. It is much higher than that of conventional metal wires and can help improve the heat exchange efficiency due to the larger contact area.

However, there are some remained issues need to be resolved in the applications of CNTs. The properties of CNTs are severely affected by the presence of defects, which are still difficult to control. Also, a wide range of thermal conductivity (1100 to 7000 W/mK) has been reported for CNTs [196], which is probably due to the difficulty in charactering the true nanotube thickness. From nano-scale single to macro-scale CNTs fibers, the efficiency in terms of power, electricity, and thermal properties is even less than 10%, which limits the engineering application of CNTs fibers [197]. In textile applications, it is still a challenge to integrate or weave CNT fibers into textiles effectively due to the limited length dependent performance and issues of compatibility with conventional textile production systems. Besides, most fabrication methods of CNTs are relatively expensive that limits the scale of utilization.

6.3. Graphene fibers

Graphene is a 2D structure array of carbon atoms with hexagonal crystalline structure and sp2 bond. [198] It emerged as a revolutionary material and has been applied in flexible electronics, optoelectronics, composite materials, energy generation and storage and sensors, etc. due to its amazing properties such as high electron mobility at room temperature, high thermal conductivity (above 5000 $W\cdot m^{-1} K^{-1}$), high Young's modulus (1 TPa), great intrinsic strength (130 GPa), impermeability to any gases, ability to sustain high electric current densities and easy chemical functionalization. Exfoliation of individual graphene sheets from graphite crystals was first realized in Geim's work through hand peeling and later on achieved by mechanical and chemical exfoliation at a large scale [199]. Individual graphene sheets were testified to possess many extraordinary properties compared with existing materials. The planar sp^2-hybridized carbon bonding promotes graphene with the maximum mechanical strength of 130 GPa and modulus of 1100 GPa in the planar direction. In addition, the long phonon mean-free-path and high phonon group velocity contributed a record high value of in-plane thermal conductivity (5300 W/mK) of suspended graphene [200,201]. Integrating graphene into textiles can not only enhance the thermal conductivity but also enable multi-functions. Graphene with a 2D topology is extremely anisotropic and most of its favorable properties are exhibited along the planar direction, such as tensile strength and thermal conducting properties because of the well-ordered arrangement of building blocks. This property is a general perquisite for high-performance targets of macro-assembled materials, especially for carbonaceous fibers. To achieve a high degree of molecular orientation in the as-spun pitch fibers, mesophase pitches with nematic liquid crystallinity [202] were commonly used as precursors, which inspires the macro-assembly of graphene sheets into fibers with continuous compact state and regular alignment.

Graphene fiber (GF), a new breed of carbonaceous fiber, starting from low-cost graphite, is directly assembled from graphene or graphene derivatives and have shown remarkable advantages from prefabrication to state-of-the-art. GF was first created by the wet spinning of graphene oxide (GO) liquid crystal (LCs) in the lab by Gao and Xu in 2011 [203]. This method has prevailed in the fabrication of GFs and has greatly extended to the production of neat, composite, hybrid GFs, in a continuous and scalable manner. The wet-spinning process of GO fibers encompasses a series of procedures involving homogenization in spinning channels, solvent exchange in a coagulation bath and post-stretching by drawing-collecting and air drying. As shown in Fig. 16a, the uniaxial shear flow occurring at the inner wall of the spinning pipe compels the GO sheets to achieve high regularity. In the coagulation bath, solvent exchange between the spinning dopes and the coagulation agent leads to the phase transition from homogeneous solution to a gel state. Suitable solvating species and binders are conductive to the oriented alignment of GO sheets in this process, resulting in freestanding and robust gel GO fibers that can endure continuous pulling and stretching. After being removed from the coagulation bath, the gel GO fibers are dried into thin fibers with compact microstructures by capillary shrinkage forces, after which GO fibers are converted into GFs by chemical and/or thermal reduction to eliminate oxygen-containing

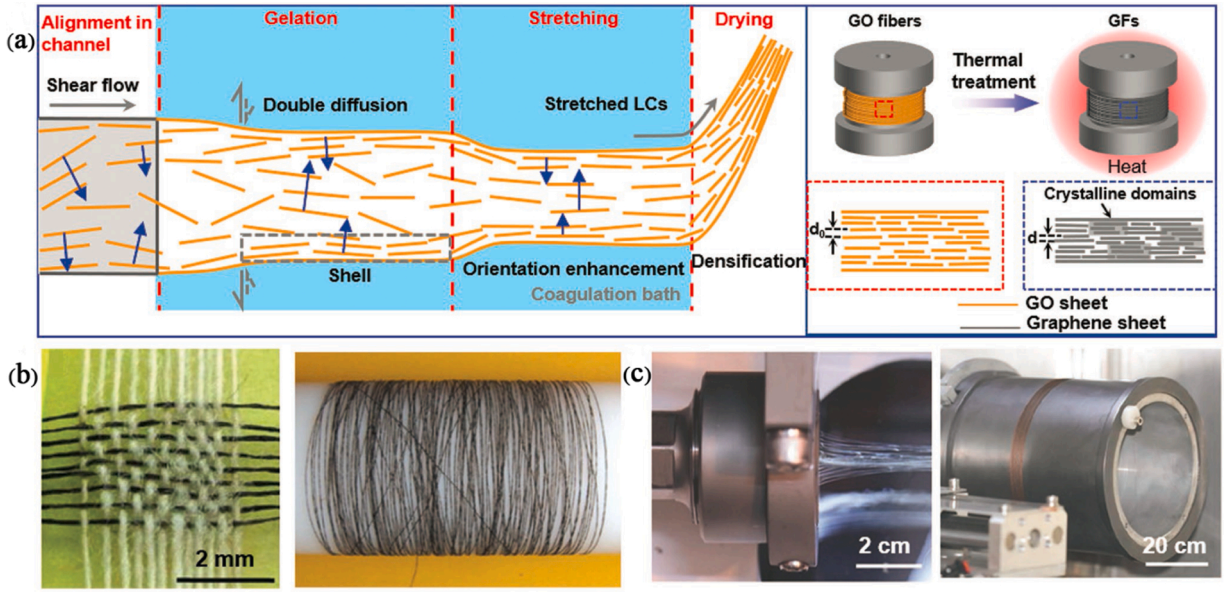

Fig. 16. (a) The schematic showing the evolution of GO fibers during wet-spinning and thermal treatment processes; (b) The SEM image of aGF-based fabric [203]; (c) A 50-filament GOF produced in a continuous manner [206].

functional groups and restore the graphene lattice. Diverse treatments have been applied to convert GO fibers into GFs, from low-temperature chemical reductions with common reducing reagents, e.g., hydroiodic acid, hydrazine hydrate, aqueous alkali, and sodium citrate, to electrothermal treatment under low bias and thermal treatment at 1000 K [204]. Chemical reduction partially removes oxygen-containing groups in GOFs, turning insulating GOFs into reduced GFs accompanied by decreased interlayer spacing, and improved mechanical strength and conducting properties. Due to the elaborate design in maximizing the sheet arrangement by shear flow and post-stretching, the wet-spinning method has been widely used to fabricate high-performance GFs. The initial wet-spun GF presents good flexibility and is capable of being woven into fabric (Fig. 16b). Some other fascinating properties, such as a high electrical conductivity of 8 × 105 S m^{-1} and a thermal conductivity of 1290 W/m-K have been achieved [205]. liquid crystal wet spinning is easily scaled up to prepare strands beyond single fibers, by using multifilament spinning nozzles. Xu et al. [206] further improved the 50-filament efficiency to 100-filament efficiency with diameters of single GF filament ranging from 1.6 to 20 μm. Combined with lengthening of the wet-spinning line and a production rate up to 300 m h^{-1}, this fabrication technology reached a considerable scale comparable to that of the industrial manufacture of carbon fibers and polymeric fibers (Fig. 16c). The obtained macroscopic materials have varying dimensions and unlimited sizes from the millimeter level to the kilometer level. GFs can also be prepared through other methods such as dry spinning [207], confined hydrothermal strategy [208], and film twisting [209]. With these methods, GFs with controllable structures and desired performances can be fabricated to form new carbonaceous fiber species for wide applications.

In terms of thermal properties, it is widely recognized that the thermal conductivity of multilayer graphene exhibits an almost linear decrement versus the number of graphene layers, in comparison to that of single-layer graphene. The main reason for this effect is that the interlayer interactions and vibrational restrictions limit the free vibration of graphene sheets, thus retarding phonon transport. This effect can also be attributed to the influence of grain boundaries. The reduction of phonon-scattering and vibrational restrictions can be addressed by achieving large-size graphitized crystals in GFs, which facilitates the phonon transportation. High-temperature treatment can heal the injured graphene sheets and promote the growth of graphitized crystalline domains. Xin et al. [205] found that the domain sizes of GFs were improved substantially from 40-50 to 783 nm upon increasing the annealing temperature from 1400 to 2850 °C. Thus, the thermal conductivity was also increased from ~300 to ~1290 W/m K. Optimizing the sheet alignment and orientation of GFs could further improve the thermal conductivity to ~1575 W/ m-K.

With improved mechanical performance and transport abilities, neat and hybrid GFs have great potential in the field of flexible and wearable devices, by virtue of the electrical and thermal conductivity, flexibility, toughness, and strength of GFs. When being introduced into textiles, GFs can bring extensive merits due to the inherently scalable production and multi-functions. Li et al. [210] proposed a wet-fusing assembly technique to fabricate nonwoven GF fabrics, where GO fibers were randomly oriented and interfused together by strong bonding. The nonwoven fabrics were highly porous and lightweight, performing high electrical conductivity (2.8 × 104 S/m) and high in-plane thermal conductivity (301.5 W/m K). The fabric made of GFs can be applied in ultrafast-responding electrothermal heaters or wearable cooling devices as a thermal transfer media. Besides, GF fabrics can be applied in energy storage devices, such as batteries and supercapacitors, which are important accessories for active thermal management methods, where extra power supply is needed, such as the wearable thermoelectric cooling system.

Today, if a multilevel hierarchy of the GF industry needs to be established, including the scalable production of GO, stable wet spinning, superb GFs, and structural-functional integrated applications. The industrialization of GFs requires bridging the gap between achievements and expectations through conquering the challenges of every step [199]. Efforts [206] including preparing high-quality raw materials, tightly controlling wet-spinning procedures, optimizing the performance and enriching the applications of GFs have been made (Fig. 17).

6.4. Boron nitride in textiles

In the recent years, advances in the synthesis of boron nitride (BN) based materials, especially those with hexagonal boron nitride structures, have attracted remarkable interests in both academic research and industrial applications, because of their low electrical conductivity and high thermal conductivity. Unlike CNTs or graphene, BN is an electrical insulator with dielectric constant 3-4, and thus can be applied in thermal management of high power electronics. The boron nitride, containing sp^2 or sp^3 bonds [211], have different allotropes from bulk to zero-dimensional, such as cubic-BN (c-BN), wurtzite-BN (w-BN), hexagonal-BN (h-BN), rhombohedral-BN (r-BN), boron nitride nanotubes (BNNT) with single or multiple walls, boronnitride nanoribbon (BNNR) with zigzag and armchair edges, boron nitride nanocages and quantum dots [212]. The thermal conductivity of conventional BN nanocomposites, however, is only around 5 W/m-K [213]. As shown in Fig. 18, a recent study demonstrated the schematic model for thermal conductivity of BN allotropes [214].

BN nanosheets, which exhibit ultrahigh thermal conductivity (2000 W m^{-1} K^{-1}), amicability to colorful dyes, excellent chemical stability, and low cost, are promising fillers for thermal conductive textiles [215]. In the past decades, researchers attempted to incorporate fiber aggregation with BN nanosheets through various processing techniques, including dip coating, wet spinning, and 3D printing [216,214]. However, these fabrics usually show low thermal conductivity due to the restricted loading rate of BN nanosheets and poor feasibility for industrialization. For instance, Zhi et al. [217] initiated the studies on polymer/BN composites for thermal conductivity enhancement, but the improvement was still insufficient. It is mainly because the poor interactions between the BN and polymers leads to high interfacial thermal resistance. Although surface functionalization of BN has been used to improve the interaction, the thermal conductivity of composites is still below 5.0 W m^{-1} K^{-1} [218]. The limitations come from the chemical inertness of BN as well as its degraded crystalline structure. Also, it is still a challenge to improve the interaction between BN and polymers without sacrificing the crystalline structure.

Most recently, electrospinning technique with fascinating characteristics of a wide range of materials, easy incorporation of additives, and remarkably low cost has been established as a simple and scalable method to fabricate BN contained thermally conductive membranes. A variety of BN nanosheets enriched nanofibrous membranes have been fabricated with different polymer templates, including polyvinylidene fluoride (PVDF) [219], polyvinylpyrrolidone (PVP) [220], and polyvinyl alcohol (PVA) [221]. Nevertheless, these membranes must undergo complex subsequent hot pressing to achieve high thermal conductivity, and thus were deprived of porous structure for moisture transportation. Yu et al. [222] reported a facile and effective strategy for scalable fabrication of thermal conductive, moisture-permeable, and superhydrophobic nanofibrous membranes via one-step electrospinning (Fig. 19). Through controlling the loading rate of BN nanosheets and ambient relative humidity, a well-interpenetrated BN network was constructed which contributed to a relatively high thermal conductivity (17.9 W/m-K) of the membrane. Meanwhile, the membrane had a hydrophobic porous structure that allowed moisture to transmit and resisted water penetration. The innovative design and multifunctional properties of the material broaden the path for the development of advanced cooling fabrics. So far, the BN is mainly applied as fillers to improve the thermal conductivity of the polymer fibers [223,224], therefore the improvement in thermal conductivity is limited. Fibers made of pure BN for higher thermal conductivity has not been reported

Fig. 17. The ideal drawing of saclable GO, superb GFs, and GF-based gloves [206].

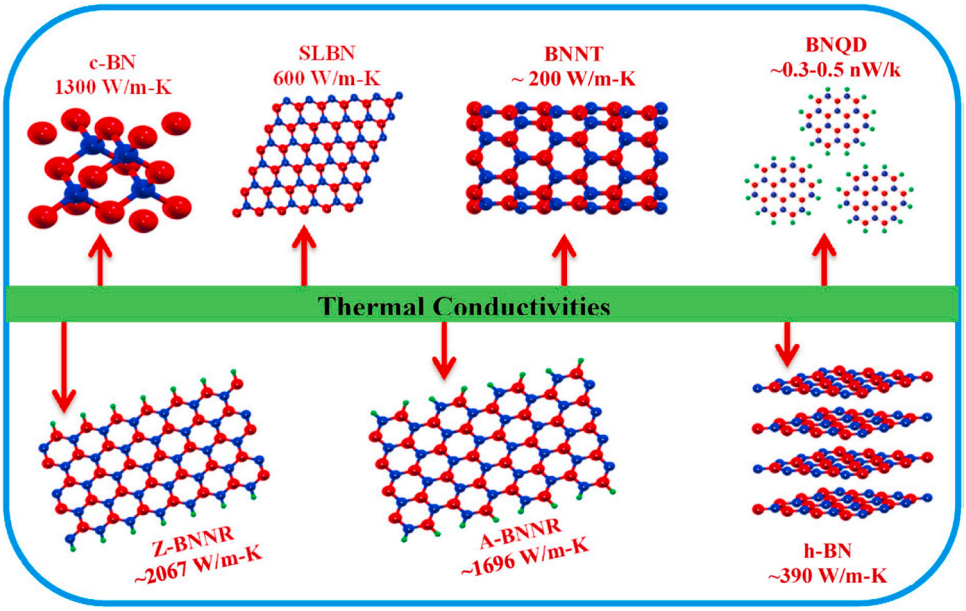

Fig. 18. Schematic model for thermal conductivity of BN allotropes. Boron nitride-based materials like BNNR, c-BN and nanotube have high thermal conductivity which hinders them to be used in their pristine form. The thermal conductivity varies from ~2000 W/m-K to ~0.3 nW/K in which nanoengineering reduces thermal conductivity significantly [212].

yet but may be possible in the future just like the preparation of graphene fibers.

6.5. Limitations and possible solutions

The thermal conductive materials (e.g. CNTs, graphene and BN) with excellent thermal conductivity have good potential in the application of personal thermal management of PPEs. However, only less than 10% heat transfer efficiency has so far been realized in bulk fibers or textiles in comparison with the heat transfer efficiency of the pure materials of CNTs, graphene and BN. Especially for textile applications, the overall thermal conductivity is limited by the porous structure. Also, the heat transfer efficiency between the cooling surface and human body is compromised by the rough surface of textiles.

To improve the continuity of textile structure and increase the overall thermal conductivity, metallic coating is commonly used to induce conductive bonding among fibers/yarns. In Ali's study [242], a conductive textile was developed with silver plating performed on the surface of a thin polyester non-woven fabric. With 21% mass ratio of silver coating, thermal conductivity of the fabric was more than 3 times higher than that of the uncoated fabric. It was also found that void space in the fabric was partially filled by silver, which resulted in a higher level of continuity for heat transfer within the fabric. With the application of metallic coating in textiles containing thermal conductive materials (e.g. CNTs, graphene and BN), it is possible to further enhance the overall thermal conductivity.

To improve the heat transfer efficiency between skin and fabric, textiles with cool-touch property [243,244] may provide a useful experience. The sensation of coolness is a transient heat conduction phenomenon when skin touchs the fabric. Usually, a smoother fabric surface feels cooler to touch because the contact area for thermal conduction is maximized, leading to a rapid heat exchange. The coolness of fabric can be influenced by different textile parameters, such as cross-section of fibers, twist level of yarns, yarn number, pore volume ratio, geometric roughness, stitch density, stiffness and weight of fabrics, etc. [245–248] In Park's study [246], the optimal combination of textile parameters for the cool-touch property of knitted fabric was investigated. Through an optimization of textile parameters, the cooling performance of thermal conductive textiles might be further improved.

7. Summary and concluding remarks

In this paper, advanced materials for use as protective clothing layers, portable cooling sources and wearable heat transfer media for the enhancement of thermal and moisture management of PPE systems are reviewed and discussed in detail, which include:

1) The ITVO (infrared transparent and visible light opaque) fabrics, which have drawn tremendous attention owing to their unique heat transport properties. The ITVO fabrics that are commonly made of nanoporous PE or other high IR transmittance polymers may be applied as protective gown layers due to the good water repellency and adjustable air permeability. Especially for indoor environments like hospitals, the room temperature allows sufficient temperature

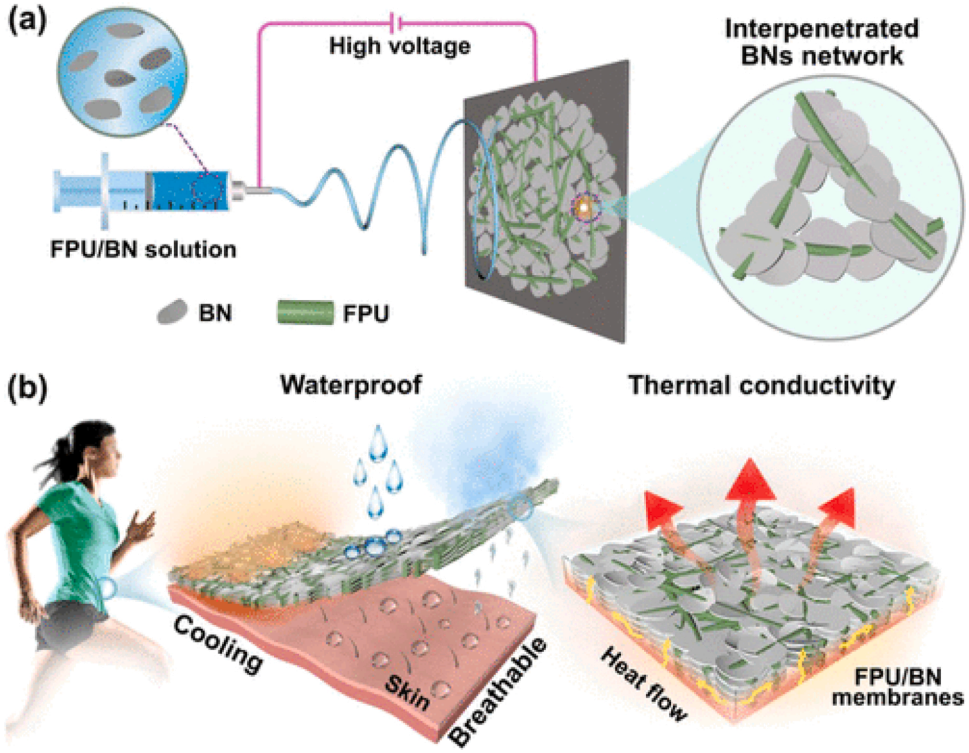

Fig. 19. (a) Schematic illustration of the fabrication and structure of BN Membranes; (b) Schematic demonstration of waterproofness, breathability, and heat conduction of BN Membranes [222].

gradient for IR radiative heat loss from human body, which can potentially relieve the heat stress caused by the generally low permeability of protective gowns.

2) The Janus or unidirectional liquid transport materials. Janus materials expel the condensed moisture from the inner layer of protective gown to the outer layer, thus reducing the relative humidity of the clothing microclimate and improving the breathability of the PPE system. The concept of Janus materials may be combined with that of the ITVO fabrics to develop infrared transparent protective layer with unidirectional water transportation properties. So far, research in this aspect is still conceptual. Further work on garment development may be promising.
3) Phase changing materials (PCMs). As a passive cold source, PCMs have been widely used for personal cooling in commercial products. Latest developments include new encapsulating methods, such as adding carbon-based continuous fillers or coaxial electrospinning, in order to improve the thermal conductivity and the adaptability to different applications. Textiles made of core-sheath PCM fibers seem more promising for wearable systems due to the high flexibility and good permeability. But it is still a challenge to balance the mechanical properties and the thermal conductivity of the polymeric sheath materials.
4) Thermoelectric (TE) systems. For more stable and controllable cooling effect, TE cooler as an active cold source show good potential for personal thermal management. With specific parametric design of TE module and appropriate combination of heat sinks, the TE system can achieve a remarkable cooling effect and stable performance in on-body use. However, the flexibility and the additional weight from the batteries may limit the application of TE coolers as wearable devices. Besides, the need for heat dissipation of TE coolers can be challenging in PPEs used in infectious environments (e.g. isolation gown).
5) Materials and devices for improved heat dissipation. To distribute the cooling effect generated from the cold sources to larger areas of human body, conventional methods include forced convection by air blowing or liquid circulation. Advanced thermally conductive materials such as carbon nanotube (CNT), graphene or Boron nitride (BN) textiles are useful for enhanced heat transfer without compromising the breathability and flexibility. The application of these materials in PPEs is seldomly reported, which could be a promising direction for future studies.

CRediT authorship contribution statement

Lun Lou: Conceptualization, Investigation, Writing - original draft, Visualization. **Kaikai Chen:** Investigation, Writing - original draft. **Jintu Fan:** Writing - review & editing, Supervision, Funding acquisition.

Declaration of Competing Interest

The authors report no declarations of interest.

Acknowledgements

We acknowledge the financial support by the Hong Kong Polytechnic University (Grant No. ZE1H), and by the Hong Kong Research Grant Council of University Grants Committee (UGC) (Ref No: 15213920).

References

[1] N. Zhu, D. Zhang, W. Wang, X. Li, B. Yang, J. Song, X. Zhao, B. Huang, W. Shi, R. Lu, P. Niu, F. Zhan, X. Ma, D. Wang, W. Xu, G. Wu, G. Gao, W. Tan, N. Engl. J. Med. 382 (2020) 727–733.
[2] https://www.cdc.gov/mmwr/volumes/69/wr/mm6915e6.htm?s_cid=mm6915e6_w.
[3] Centers of Disease Control and Prevention (CDC), Scientific Brief: SARS-CoV-2 and potential airborne transmission, 2020. October 5, https://www.cdc.gov/coronavirus/2019-ncov/more/scientific-brief-sars-cov-2.html.
[4] https://www.ecdc.europa.eu/en/publications-data/guidance-wearing-and-removing-personal-protective-equipment-healthcare-settings.
[5] N. Karim, S. Afroj, K. Lloyd, L.C. Oaten, D.V. Andreeva, C. Carr, A.D. Farmery, I. D. Kim, K.S. Novoselov, ACS Nano 14 (2020) 12313–12340.

[6] https://www.fda.gov/medical-devices/personal-protective-equipment-infection-control/medical-gowns.
[7] V. Parthasarathi, G. Thilagavathi, J. Text. Inst. 106 (2015) 1095–1105.
[8] F.S. Kilinc, J. Eng. Fibers Fabr. 10 (2015) 180–190.
[9] E. Vozzola, M. Overcash, E. Griffing, AORN J. 111 (2020) 315–325.
[10] S. Aslan, S. Kaplan, C. Cetin, J. Text. I. 104 (2013) 870–882.
[11] W.A. Rutala, D.J. Weber, Infect. Cont. Hosp. Ep. 22 (2001) 248–257.
[12] T. Quinn, J.H. Kim, Y. Seo, A. Coca, Prehosp. Disaster Med. 33 (2018) 279–287.
[13] T. Quinn, J.H. Kim, A. Strauch, T. Wu, J. Powell, R. Roberge, R. Shaffer, A. Coca, Disaster Med. Public Health Prep. 11 (2017) 573–579.
[14] D.S. Chertow, C. Kleine, J.K. Edwards, R. Scaini, R. Giuliani, A. Sprecher, N. Engl. J. Med. 371 (2014) 2054–2057.
[15] R.N. Anja, N. Wolz, Engl. J. Med. 371 (2014) 1081–1083.
[16] C. Gao, Phase-change materials (PCMs) for warming or cooling in protective clothing. Protective Clothing, Woodhead Publishing, 2014.
[17] C. Chou, Y. Tochihara, T. Kim, Eur. J. Appl. Physiol. 104 (2008) 369–374.
[18] J.P. Dionne, K. Semeniuk, A. Makris, W. Teal, B. Laprise, Thermal manikin evaluation of liquid cooling garments intended for use in hazardous waste management, in: WM'03 Conference, Tucson, AZ, 2003.
[19] J.H. Kim, A. Coca, W.J. Williams, R.J. Roberge, Ergonomics 54 (2011) 626–635.
[20] A.D. Flouris, S.S. Cheung, Ann Biomed Eng 34 (2006) 359.
[21] National Urban Security Technology Laboratory, Personal cooling systems market survey report, 2016.
[22] L. Lou, Y.S. Wu, D. Shou, J. Fan, Annual Rev. Heat Transfer 21 (2019) 205–244.
[23] W. Song, F. Wang, Ergonomics 59 (2016) 1009–1018.
[24] T.D. Chinevere, Eur. J. Appl. Physiol. 103 (2008) 307–314.
[25] D. Zhao, X. Lu, T. Fan, Y.S. Wu, L. Lou, Q. Wang, J. Fan, R. Yang, Applied Energy 218 (2018) 282–291.
[26] R. Williamson, J. Carbo, B. Luna, B.W. Webbon, J Occup Environ Med. 41 (1999) 453–463.
[27] B.S. Cadarette, L. Levine, J.E. Staab, M.A. Kolka, M.M. Correa, M. Whipple, M. N. Sawka, AIHA J. 64 (2003) 510–515.
[28] N. Djongyang, R. Tchinda, D. Njomo, Renew. Sustain. Energy Rev. 14 (2010) 2626–2640.
[29] H. Zhou, Z. Guo, J. Mater. Chem. A 7 (2019) 12921.
[30] H. Li, J. Yang, Z. Xu, Adv. Mater. Interfaces 7 (2020), 1902064.
[31] C.K. Soz, S. Trosien, M. Biesalski, ACS Materials Lett. 2 (2020) 336–367.
[32] H. Wang, H. Zhou, H. Niu, J. Zhang, Y. Du, T. Lin, Adv. Mater. Interfaces 2 (2015), 1400506.
[33] H. Wang, H. Zhou, W. Yang, Y. Zhao, J. Fang, T. Lin, ACS Appl. Mater. Interfaces 7 (2015) 22874–22880.
[34] N. Wang, Y. Yang, S.S. Al-Deyab, M. El-Newehy, J. Yu, B. Ding, J. Mater. Chem. A 3 (2015) 23946.
[35] S. Zhang, H. Liu, J. Yu, W. Luo, B. Ding, J. Mater. Chem. A 4 (2016) 6149.
[36] X. Li, N. Wang, G. Fan, J. Yu, J. Gao, G. Sun, B. Ding 439 (2015) 12–20.
[37] Z. Zhong, Z. Xu, T. Sheng, J. Yao, W. Xing, Y. Wang, ACS Appl. Mater. Interfaces 7 (2015) 21538–21544.
[38] N. Vitchuli, Q. Shi, J. Nowak, K. Kay, J.M. Caldwell, F. Breidt, M. Bourham, M. McCord, X. Zhang, Sci. Technol. Adv. Mater. 12 (2011), 055004.
[39] A. Baji, Y. Mai, Q. Li, Y. Liu, Compos. Sci. Technol. 71 (2011) 1435–1440.
[40] X. Zhao, Y. Li, T. Hua, P. Jiang, X. Yin, J. Yu, B. Ding, Small 13 (2017), 1603306.
[41] J. Wu, N. Wang, L. Wang, H. Dong, Y. Zhao, L. Jiang, Soft Matter 8 (2012) 5996.
[42] Y. Dong, J. Kong, S.L. Phua, C. Zhao, N.L. Thomas, X. Lu, ACS Appl. Mater. Interfaces 6 (2014) 14087–14095.
[43] Y. Dong, J. Kong, C. Mu, C. Zhao, N.L. Thomas, X. Lu, Materials and Design 88 (2015) 82–87.
[44] D. Miao, Z. Huang, X. Wang, J. Yu, B. Ding, Small 14 (2018), 1801527.
[45] D. Shou, J. Fan, Adv. Funct. Mater. 28 (2018), 1800269.
[46] H. Zhou, H. Wang, H. Niu, T. Lin, Scientific Reports 3 (2013) 2964.
[47] L. Huang, S.S. Manickam, J.R. McCutcheon, Journal of Membrane Science 436 (2013) 213–220.
[48] K. Ho, L. Lin, S. Weng, K. Chuang, Science of the Total Environment 735 (2020), 139510.
[49] X. Tian, H. Jin, J. Sainio, R.H.A. Ras, O. Ikkala, Adv. Funct. Mater. 24 (2014) 6023–6028.
[50] H. Liu, J. Huang, F. Li, Z. Chen, K. Zhang, S.S. Al-Deyab, Y. Lai, Cellulose 24 (2017) 1129–1141.
[51] F.S. Kilinc, J. Eng, Fiber Fabr. 10 (2015) 180–190.
[52] Y. Kong, Y. Liu, J.H. Xin, J. Mater. Chem. 21 (2011) 17978.
[53] L. Lao, D. Shou, Y.S. Wu, J.T. Fan, Sci. Adv. 6 (2020) eaaz0013.
[54] H. Yang, J. Hou, L. Wan, V. Chen, Z. Xu, Adv. Mater. Interfaces 3 (2016), 1500774.
[55] H. Wang, J. Ding, L. Dai, X. Wang, T. Lin, J. Mater, Chem. 20 (2010) 7938–7940.
[56] J.D. Hardy, E.F. Dubois, PNAS 23 (1937) 624–631.
[57] C.E.A. Winslow, L.P. Herrington, A.P. Gagge, Am. J. Physiol. 127 (1939) 505.
[58] J. Steketee, Phys. Med. Biol. 18 (1973) 686–694.
[59] B. Das, A. Das, V.K. Kothari, R. Fanguiero, M. de Araujo, Fibers Polym. 9 (2008) 225–231.
[60] L. Cai, Y.A.Y. Song, W. Li, P. Hsu, D. Lin, P.B. Catrysse, Y. Liu, Y. Peng, J. Chen, H. Wang, J. Xu, A. Yang, S. Fan, Y. Cui, Adv. Mater. 30 (2018), 1802152.
[61] J.K. Tong, X. Huang, S.V. Boriskina, J. Loomis, Y. Xu, G. Chen, ACS Photonics 2 (2015) 769–778.
[62] P. Hsu, A.Y. Song, P.B. Catrysse, C. Liu, Y. Peng, J. Xie, S. Fan, Y. Cui, Science 353 (2016) 1019–1023.
[63] Y. Song, R. Ma, L. Xu, H. Huang, D. Yan, J. Xu, G. Zhong, J. Lei, Z. Li, ACS Appl. Mater. Interfaces 10 (2018) 41637–41644.
[64] A. Yang, L. Cai, R. Zhang, J. Wang, P. Hsu, H. Wang, G. Zhou, J. Xu, Y. Cui, Nano Lett. 17 (2017) 3506–3510.
[65] J.K. Tong, X. Huang, S.V. Boriskina, J. Loomis, Y. Xu, G. Chen 2 (2015) 769–778.
[66] P. Hsu, C. Liu, A.Y. Song, Z. Zhang, Y. Peng, J. Xie, K. Liu, C. Wu, P.B. Catrysse, L. Cai, S. Zhai, A. Majumdar, S. Fan, Y. Cui, Sci. Adv. 3 (2017), e1700895.
[67] ASTM G173-03, ASTM International, 2012.
[68] M. Matsuoka, Infrared Absorbing Dyes, Springer, 2013.
[69] J. Lee, M.H. Kang, K.B. Lee, Y. Lee, Materials 6 (2013) 2007–2025.
[70] T. Kim, S. Jeon, D. Kwak, Y. Chae, Fibers Polym. 13 (2012) 212–216.
[71] M. Nardin, I.M. Ward, Mater. Sci. Technol. 3 (1987) 814–826.
[72] L. Cai, Y. Peng, J. Xu, C. Zhou, C. Zhou, P. Wu, D. Lin, S. Fan, Y. Cui, Joule 3 (2019) 1478–1486.
[73] N. Pan, Global Challenges 3 (2019), 1800082.
[74] S. Ye, Q. Zhang, D. Hu, J. Feng, J. Mater. Chem. A 3 (2015) 4018.
[75] Https://Www.Nasa.Gov/Pdf/413410main_Phasechange.Pdf.
[76] L. Lou, Y.S. Wu, D. Shou, J. Fan, Annual Reviews of Heat Transfer 21 (2019) 205–244.
[77] National Urban Security Technology Laboratory, Personal cooling systems market survey report, 2016.
[78] J. Smolander, K. Kuklane, D. Gavhed, H. Nillson, I. Holmer, JOSE 10 (2004) 111–117.
[79] B.L. Bennett, R.D. Hagan, K.A. Huey, C. Minson, D. Cain, Eur. J. Appl. Physiol. Occup. Physiol. 70 (1995) 322–328.
[80] M. Buhler, A.M. Popa, L.J. Scherer, F.K.S. Lehmeier, R.M. Rossi, Appl. Therm. Eng. 54 (2013) 359.
[81] F. Salaun, E. Devaux, S. Bourbigot, P. Rumeau, Text. Res. J. 80 (2009) 195–205.
[82] H. Shim, E.A. Mccullough, B.W. Jones, Text. Res. J. 71 (2001) 495–502.
[83] H. Yoo, J. Lim, E. Kim, Text. Res. J. 83 (2013) 671–682.
[84] J. L. Zuckerman, R. J. Pushaw, B. T. Perry, D. M. Wyner, US Patent 6514362 (2003).
[85] D. Feldman, M.M. Shapiro, D. Banu, C.J. Fuks, Solar Energy Materials 18 (1989) 201–216.
[86] D.G. Prajapati, B. Kandasubramanian, Polymer Reviews 60 (2020) 389–419.
[87] C. Gao, K. Kuklane, F. Wang, I. Holmer, Indoor Air 22 (2012) 523–530.
[88] A. Saito, S. Okawa, T. Shintani, R. Iwamoto, Int. J. Heat Mass Transf. 44 (2001) 4693–4701.
[89] S.A. Arngrimsson, D.S. Petitt, M.G. Stueck, D.K. Jorgensen, K.J. Cureton, Journal of Applied Physiology 96 (2004) 1867–1874.
[90] S. Mondal, Applied Thermal Engineering 28 (2008) 1536–1550.
[91] M. Malekipirbazari, S.M. Sadrameli, F. Dorkoosh, H. Sharifi, Int. J. Energy Res. 38 (2014) 1492–1500.
[92] M.N.A. Hawlader, M.S. Uddin, M.M. Khin, Appl. Energy 74 (2003) 195–202.
[93] K. Sun, Y. Kou, H. Zheng, X. Liu, Z. Tan, Q. Shi, Sol. Energy Mater. Sol. Cells 178 (2018) 139–145.
[94] S. Lu, T. Shen, J. Xing, Q. Song, J. Shao, J. Zhang, C. Xin, Mater. Lett. 211 (2018) 36–39.
[95] A. Elgafy, K. Lafdi, Carbon 43 (2005) 3067–3074.
[96] Z. Han, A. Fina, Prog. Polym. Sci. 36 (2011) 914–944.
[97] Z. Qiao, J. Mao, Journal of Microencapsulation 34 (2017) 1–9.
[98] J. Shi, M. Ger, Y. Liu, Y. Fan, N. Wen, C. Lin, N. Pu, Carbon 51 (2013) 365–372.
[99] D.G. Atinafu, W. Dong, C. Wang, G. Wang, J. Mater. Chem. A 6 (2018) 8969.
[100] B. Li, T. Liu, L. Hu, Y. Wang, S. Nie, Chem. Eng. J. 215 (2013) 819–826.
[101] J. Li, W. Lu, Y. Zeng, Z. Luo, Sol. Energy Mater. Sol. Cells 128 (2014) 48–51.
[102] Y. Zhong, M. Zhou, F. Huang, T. Lin, D. Wan, Sol. Energy Mater. Sol. Cells 113 (2013) 195–200.
[103] L. Chen, R. Zou, W. Xia, Z. Liu, Y. Shang, J. Zhu, Y. Wang, J. Lin, D. Xia, A. Cao, ACS Nano 6 (2012) 10884–10892.
[104] H. Ji, D. Sellan, M. Pettes, X. Kong, J. Ji, L. Shi, R. Ruoff, Energy Environ. Sci. 7 (2014) 1185–1192.
[105] F. Wang, C. Gao, K. Kuklane, I. Holmer, JOSE 16 (2010) 387–404.
[106] X. Tao, Handbook of Smart Textiles, Springer, 2016.
[107] A. Nejman, M. Cieslak, B. Gajdzicki, B.G. Grabowska, A. Karaszewska, Thermochimica Acta 589 (2014) 158–163.
[108] C. Gao, K. Kuklane, I. Holmer. Proceedings of the 7th International Thermal Manikin and Modelling Meeting, 2008.
[109] K. Iqbal, D. Sun, Cellulose 25 (2018) 2103–2113.
[110] A.G. Hassabo, A.L. Mohamed, Carbohydr. Polym. 165 (2017) 421–428.
[111] A. Nejman, M. Cieslak, Appl. Therm. Eng. 127 (2017) 212–223.
[112] A.B. Rezaie, M. Montazer, Appl. Energy 228 (2018) 1911–1920.
[113] S.I. Golestaneh, G. Karimi, A. Babapoor, F. Torabi, Appl. Energy 212 (2018) 552–564.
[114] W. Chen, W. Weng, Appl. Energy 173 (2016) 168–176.
[115] R. Faridi-Majidi, M. Madani, N. Sharifi-Sanjani, S. Khoee, A. Fotouhi, Polym Plast Technol Eng 51 (2012) 364–368.
[116] A. Babapoor, G. Karimi, S.I. Golestaneh, M.A. Mezjin, Appl. Therm. Eng. 118 (2017) 398–407.
[117] D.G. Prajapati, B. Kandasubramanian, Polymer Reviews 60 (2020) 389–419.
[118] F. Haghighat, S.A.H. Ravandi, M.N. Esfahany, A. Valipouri, J. Mater. Sci. 53 (2018) 4665–4682.
[119] Y. Lu, X. Xiao, Y. Zhan, C. Huan, S. Qi, H. Cheng, G. Xu, ACS Appl. Mater. Interfaces 10 (2018) 12759–12767.
[120] C.L. Choy, Polymer 18 (1977) 984–1004.
[121] Y. Lu, F. Wei, D. Lai, W. Shi, F. Wang, C. Gao, G. Song, Journal of Thermal Biology 52 (2015) 137–146.
[122] M. Itani, N. Ghaddar, K. Ghali, Energy Convers. Manag. 140 (2017) 218–227.
[123] M. Itani, R. Bachnak, N. Ghaddar, K. Ghali, J. Build. Eng. 22 (2019) 383–396.

[124] L.E. Dorman, G. Havenith, J. Appl. Physiol. 105 (2009) 463–470.
[125] J.C.A. Peltier, Ann. Chim. Phys. 56 (1823) 371–386.
[126] E. Lenz, Analen der Physik 120 (1838) 342–349.
[127] G. Magnus, Ann. Der Phys. Und Chemie 83 (1851) 469–504.
[128] W. Thomson, Math. Phys. Pap. 1 (1851) 175–183.
[129] R.A. Kishore, A. Nozariasbmarz, B. Poudel, M. Sanghadasa, S. Priya, Nat. Commun 10 (2019) 1765.
[130] A. Attar, H. Lee, Energy Conv Manag 112 (2016) 328–336.
[131] X. Hao, B. Peng, G. Xie, Y. Chen, Appl Therm Eng 100 (2016) 170–178.
[132] N. Putra, S.W. Ardiyansyah, D. Johansen, F.N. Iskandar, Cryogenics 50 (2010) 759–764.
[133] D. Beretta, N. Neophytou, J.M. Hodges, M.G. Kanatzidis, D. Narducci, M. Martin-Gonzalez, M. Beekman, B. Balke, G. Cerretti, W. Tremel, A. Zevalkink, A. I. Hofmann, C. Muller, B. Dorling, M. Compoy-Quiles, M. Caironi, Mater. Sci. Eng. R Rep 138 (2019) 210–255.
[134] D. Zhao, X. Lu, T. Fan, Y.S. Wu, L. Lou, Q. Wang, J. Fan, R. Yang, Appl Energy 218 (2018) 282–291.
[135] S. Hong, Y. Gu, J.K. Seo, J. Wang, P. Liu, Y.S. Meng, S. Xu, R. Chen, Sci. Adv. 5 (2019) eaaw0536.
[136] A.F. Ioffe, Semiconductor Thermoelements, and Thermoelectric Cooling, Infosearch, London, 1957.
[137] F.J. DiSalvo, Science 285 (1999) 459–539.
[138] H.J. Goldsmid, A.R. Sheard, D.A. Wright, Br. J. Apply. Phys. 9 (1958) 365–370.
[139] H.J. Goldsmid, J. Appl. Phys. 32 (1961) 2198–2202.
[140] W. Liu, K.C. Lukas, K. McEnaney, S. Lee, Q. Zhang, C.P. Opeil, G. Chen, Z. Ren, Energy Environ. Sci. 6 (2013) 552.
[141] S. Kim, K.H. Lee, H.A. Mun, H.S. Kim, S.W. Hwang, J.W. Roh, D.J. Yang, W. H. Shin, X.S. Li, Y.H. Lee, G.J. Snyder, S.W. Kim, Science 348 (2015) 109–114.
[142] F. Suarez, A. Nozariasbmarz, D. Vashaee, M.C. Ozturk, Energy Environ. Sci. 9 (2016) 2099–2113.
[143] M.L. Cohen, A review J. Invest. Dermatol. 69 (1977) 333–338.
[144] P.D. Richardson, J.H. Whitelaw, J. Franklin Inst. 286 (1968) 169–181.
[145] X. Lu, D. Zhao, T. Ma, Q. Wang, J. Fan, R. Yang, Energy Conv Manag 169 (2018) 186–193.
[146] H.S. Lee, Appl Energy 106 (2013) 79–88.
[147] D.K. Kim, S.J. Kim, J.K. Bae, Int. J. Heat Mass Transf. 52 (2009) 3510–3517.
[148] Y.M. Seo, M.Y. Ha, S.H. Park, G.H. Lee, Y.S. Kim, Y.G. Park, Appl Therm Eng 128 (2018) 1082–1094.
[149] Y. Zhou, J. Yu, Int J Refrig 35 (2012) 1139–1144.
[150] L. Zhu, H. Tan, J. Yu, Energy Conv Manag 76 (2013) 685–690.
[151] L. Zhu, J. Yu, Int J Therm Sci 118 (2017) 168–175.
[152] L. Lou, D. Shou, H. Park, D. Zhao, Y.S. Wu, X. Hui, R. Yang, E.C. Kan, J. Fan, Energy & Buildings 226 (2020), 110374.
[153] J.A. Greenwood, J.B.P. Williamson, Proc R Soc A: Math Phys Eng Sci. 295 (1966) 300–319.
[154] K.M. Razeeb, E. Dalton, G.L.W. Cross, A.J. Robinson, Int. Mater. Rev. 63 (1) (2018) 1–21.
[155] P. Lv, X.W. Tan, K.H. Yu, R.L. Zheng, J.J. Zheng, W. Wei, Carbon 99 (2016) 222–228.
[156] Q.Z. Liang, X.X. Yao, W. Wang, Y. Liu, C.P. Wong, ACS Nano 5 (2011) 2392–2401.
[157] R.J. Warzoha, D. Zhang, G. Feng, A.S. Fleischer, Carbon 61 (2013) 441–457.
[158] C.K. Roy, S. Bhavnani, M.C. Hamilton, R.W. Johnson, J.L. Nguyen, R.W. Knight, D.K. Harris, Int. J. Heat Mass Transfer 85 (2015) 996–1002.
[159] B. Feng, F. Faruque, P. Bao, A.T. Chien, S. Kumar, G.P. Peterson, Appl. Phys. Lett. 102 (2013), 093105.
[160] M.T. Barako, S. Roy-Panzer, T.S. English, T. Kodama, M. Asheghi, T.W. Kenny, K. E. Goodson, ACS Appl. Mater. Interfaces 7 (2015) 19251–19259.
[161] M. Shtein, R. Nadiv, M. Buzaglo, K. Kahil, O. Regev, Chem. Mater. 27 (2015) 2100–2106.
[162] M.A. Raza, A.V.K. Westwood, C. Stirling, R. Ahmad, Composites Science and Technology 120 (2015) 9–16.
[163] K.M.F. Shahil, A.A. Balandin, Nano Lett. 12 (2012) 861–867.
[164] N. Karwa, C. Stanley, H. Intwala, G. Rosengarten, Applied Thermal Engineering 111 (2017) 1596–1602.
[165] P.C. Hsu, A.Y. Song, P.B. Catrysse, Science 353 (2016) 1019–1023.
[166] P.C. Hsu, C. Liu, A.Y. Song, Science advances 3 (2017), e1700895.
[167] A. Cao, J. Qu, Int. J. Appl. Phys. 112 (2012), 013503.
[168] C. Journet, W.K. Maser, P. Bernier, Nature 388 (1997) 756–758.
[169] C.D. Scott, S. Arepalli, P. Nikolaev, Applied Physics A 72 (2001) 573–580.
[170] J. Kong, A.M. Cassell, H. Dai, Chemical Physics Letters 292 (1998) 567–574.
[171] G.Z. Chen, X. Fan, A. Luget, Journal of Electroanalytical Chemistry 446 (1998) 1–6.
[172] D. Laplaze, P. Bernier, W.K. Maser, Carbon 36 (1998) 685–688.
[173] R.H. Baughman, A.A. Zakhidov, W.A. de Heer, Science 297 (2002) 787–792.
[174] W. Lu, M. Zu, J. Byun, B. Kim, T. Chou, Advanced Materials 24 (2012) 1805–1833.
[175] Y. Shang, X. He, Y. Li, Advanced Materials 24 (2012) 2896–2900.
[176] S. Shekhar, P. Stokes, S.I. Khondaker, ACS Nano 5 (2011) 1739–1746.
[177] M. Puttegowda, S.M. Rangappa, M. Jawaid, Woodhead Publishing 11 (2018) 315–351.
[178] B.C. Goswami, R.D. Anandjiwala, D. Hall, Textile sizing, CRC press, 2004.
[179] N. Behabtu, C.C. Young, D.E. Tsentalovich, O. Kleinerman, Science 339 (2013) 182–186.
[180] K. Jiang, Q. Li, S. Fan, Nature 419 (2002) 801.
[181] H.W. Zhu, C.L. Xu, D.H. Wu, B.Q. Wei, R. Vajtai, P.M. Ajayan, Science 296 (2002) 884–886.
[182] M. Zhang, S. Fang, A.A. Zakhidov, S.B. Lee, A.E. Aliev, C.D. Williams, K. R. Atkinson, R.H. Baughman, Science 309 (2005) 1215–1219.
[183] M.D. Lima, S. Fang, X. Lepró, Science 331 (2011) 51–55.
[184] J.A. Lee, Y.T. Kim, G.M. Spinks, D. Suh, X. Lepro, M.D. Lima, R.H. Baughman, S. J. Kim, Nano Letters 14 (2014) 2664–2669.
[185] X. Chen, L. Qiu, J. Ren, Advanced Materials 25 (2013) 6436–6441.
[186] J. Ren, Y. Zhang, W. Bai, Angewandte Chemie 126 (2014) 7998–8003.
[187] R. Li, X. Xiang, X. Tong, Advanced Materials 27 (2015) 3831–3835.
[188] D. Zhang, M. Miao, H. Niu, ACS Nano 8 (2014) 4571–4579.
[189] W. Weng, Q. Sun, Y. Zhang, Nano Letters 14 (2014) 3432–3438.
[190] Z. Zhang, Z. Yang, Z. Wu, Advanced Energy Materials 4 (2014), 1301750.
[191] DexMat, http://dexmat.com.
[192] Nanocomp Technologies Inc., http://www.nanocomptech.com.
[193] Lintec-NSTC, http://www.lintec-nstc.com.
[194] Suzhou Creative Nano-Carbon Co. Ltd., http://www.jdnm.com.cn.
[195] J.J. Vilatela, R. Marcilla, Chemistry of Materials 27 (2015) 6901–6917.
[196] A.A. Balandin, Nature Materials 10 (2011) 569–581.
[197] R.H. Fang, A.V. Kroll, W. Gao, L. Zhang, Adv Mater. 30 (2018), e1706759.
[198] A.K. Geim, Science 324 (5934) (2009) 1530–1534.
[199] K.S. Novoselov, A.K. Geim, S.V. Morozov, D. Jiang, Y. Zhang, S.V. Dubonos, I. V. Grigorieva, A.A. Firsov, Science 306 (2004) 666–669.
[200] D.S. Ghosh, I. Calizo, D. Teweldebrhan, E.P. Pokatilov, D.L. Nika, A.A. Balandin, W. Bao, F. Miao, C.N. Lau, Appl. Phys. Lett. 92 (2008), 151911.
[201] A.A. Balandian, S. Ghosh, W. Bao, I. Calizo, D. Teweldebrhan, F. Miao, C. Lau, Nano Lett. 8 (2008) 902–907.
[202] J.E. Kim, T.H. Han, S.H. Lee, Angewandte Chemie 123 (2011) 3099–3103.
[203] Z. Xu, C. Gao, Nature Communications 2 (2011) 571.
[204] H. Cheng, C. Hu, Y. Zhao, NPG Asia Materials 6 (2014) e113.
[205] G. Xin, T. Yao, H. Sun, S.M. Scott, D. Shao, G. Wang, J. Lian, Science 349 (2015) 1083–1087.
[206] Z. Xu, Y. Liu, X. Zhao, Advanced Materials 28 (2016) 6449–6456.
[207] Q. Tian, Z. Xu, Y. Liu, Nanoscale 9 (2017) 12335–12342.
[208] Z. Dong, C. Jiang, H. Cheng, Advanced Materials 24 (2012) 1856–1861.
[209] Z. Zhang, D. Zhang, H. Lin, Journal of Power Sources 433 (2019), 226711.
[210] Z. Li, Z. Xu, Y. Liu, R. Wang, C. Gao, Nature Communication 7 (2016) 13684.
[211] M.I. Petrescu, M.G. Balint, UPB Sci. Bull., Series B 69 (2007) 35–42.
[212] R. Arenal, A. Lopez-Bezanilla, Wiley Interdiscip. Rev. Comput. Mol. 5 (2015) 299–309.
[213] W.L. Song, P. Wang, L. Cao, Angewandte Chemie 124 (2012) 6604–6607.
[214] J. Joy, E. George, P. Haritha, Journal of Polymer Science 58 (2020) 3115–3141.
[215] C. Lei, K. Wu, L. Wu, W. Liu, R. Du, F. Chen, Q. Fu, Journal of Materials Chemistry A 7 (2019) 19364–19373.
[216] W. Luo, Y. Wang, E. Hitz, Advanced Functional Materials 27 (2017), 1701450.
[217] C. Zhi, Y. Bando, T. Terao, Advanced Functional Materials 19 (2009) 1857–1862.
[218] X. Huang, C. Zhi, P. Jiang, Advanced Functional Materials 23 (2013) 1824–1831.
[219] J. Zahirifar, A. Hadi, J. Karimi-Sabet, Desalination 460 (2019) 81–91.
[220] S. Currie, F.J. Shariatzadeh, H. Singh, ACS Applied Materials & Interfaces 12 (2020) 45859–45872.
[221] W.L. Song, P. Wang, L. Cao, Angewandte Chemie 124 (2012) 6604–6607.
[222] X. Yu, Y. Li, X. Wang, Y. Si, J. Yu, B. Ding, ACS Appl. Mater. Interfaces 12 (2020) 32078–32089.
[223] J. Chen, X. Huang, B. Sun, ACS Nano 13 (2018) 337–345.
[224] X. Zeng, J. Sun, Y. Yao, ACS Nano 11 (2017) 5167–5178.
[225] P. Xu, Z. Kang, F. Wang, Udayraj, Int. J. Environ. Res. Publich Health 17 (2020) 4995.
[226] M. Itani, N. Ghaddar, K. Ghali, D. Ouahrani, W. Chakroun, Energy and Building 138 (2017) 417–425.
[227] R. Taherian, Journal of Power Sources 265 (2014) 370–390.
[228] H. Liu, J. Li, L. Chen, L. Liu, Y. Li, X. Li, X. Li, H. Yang, Text. Res. J. 86 (2016) 1398–1412.
[229] B. Batcheller, K. Brekkestran, R. Minch, US Patent 5032705, 1989.
[230] M. Honarvar, M. Latifi, The Journal of the Textile Institute 108 (2017) 631–652.
[231] S. Omar, A. Goel, Colourage 56 (2009) 93–105.
[232] M. Pamela, F. Iwona, M. Marcin, Fibres & Textiles in Eastern Europe 28 (2020) 103–109.
[233] P. Pavvandy, M. Latifi, M. Agha-Mirsalim, J. Shokrolahi-Moghani, The Journal of The Textile Institute 101 (2010) 514–519.
[234] K. Brekkestran, K. Aghai-Tabriz, N. Nguyen, B. Batcheller, US Patent 5105067, 1989.
[235] Y. Ren, J. Gong, R. fu, Z. Li, Z. Yu, J. Lou, F. Wang, J. Zhang, 148 (2017) 375 – 385.
[236] L. Liu, Y. Yu, C. Yan, K. Li, Z. Zheng, Nature Communications 6 (2015) 7260.
[237] J. Xie, Y. Jia, M. Miao, Smart Materials and Structures 28 (2019), 035017.
[238] I. Nuramdhani, M. Jose, P. Samyn, P. Adriaensens, B. Malengier, W. Deferme, G. Mey, L. Langenhove, Polymers 11 (2019) 345.
[239] Y. Wang, W. Yu, F. Wang, Textile Research Journal 89 (2017) 487–497.
[240] S. Gao, R. Sun, Y. Feng, J. Hao, Thermal Science 25 (2021) 2289–2293.
[241] A. Quye, Polymer Degradation and Stability 107 (2014) 210–218.
[242] A. Ali, V. Baheti, J. Militky, Z. Khan, G. Zhu, Fibers and Polymers 20 (2019) 1347–1359.
[243] S. Kaplan, A. Okur, Journal of Sensory Studies 24 (2009) 479–497.
[244] F. Rombaldoni, R. Demichelis, G. Mazzuchetti, Journal of Sensory Studies 25 (2010) 899–916.
[245] A. Schneider, B. Holcombe, L. Stephens, Textile Research Journal 61 (1991) 488–494.

[246] J. Park, H. Yoo, K. Hong, E. Kim, Textile Research Journal 88 (2017) 1931–1942.
[247] R. Masood, H. Jamshaid, M. Khubaib, J. Therm. Anal. Calorim. 139 (2019) 159–167.
[248] N. Ozdil, A. Marmarali, S. Kretzschmar, Int. J. Therm. Sci. 46 (2007) 1318–1322.

Lun Lou received his Ph.D. in Fiber Science at Cornell University, NY, USA in 2019, M.S. in Materials Science and Engineering at University of Florida, FL, USA in 2015 and B.E. in Textile Engineering at Donghua University, Shanghai, China in 2012. He joined Professor Jintu Fan's group at Institute of Textiles & Clothing in The Hong Kong Polytechnic University as a postdoctoral researcher in 2020. His research focus on personal thermal and moisture management, heat and mass transfer, clothing thermal comfort and textile materials.

Kaikai Chen received his Ph.D. in Textile Science and Engineering at Tiangong University in 2019. Then he joined Prof. Jintu Fan's lab at the Institute of Textiles and Clothing in the Hong Kong Polytechnic University and became a postdoctoral researcher in 2020. His current research involves preparation and application of thermal conductive fiber. He is broadly interested in carbon nanomaterials for electronics, optoelectronics, energy, and biotechnology.

Jintu Fan is currently Chair Professor and Head of Institute of Textiles and Clothing (ITC), Hong Kong Polytechnic University (PolyU). He holds BSc from Donghua University, China and PhD and DSc from The University of Leeds, UK. He served ITC as Assistant Professor, Associate Professor, Full Professor and Associate Head from 1996 to 2012. He then joined Cornell University as Chair and Vincent V. C. Woo Professor of the Department of Fiber Science and Apparel Design in the College of Human Ecology, where he orchestrated the establishment of the Cornell Institute of Fashion & Fiber Innovation and was the founding Director of the institute. He returned to PolyU in 2018.